Research

Synthesis, in-vitro and in-silico antibacterial and computational studies of selected thiosemicarbazone-benzaldehyde derivatives as potential antibiotics

Adesoji A. Olanrewaju[1] · David G. Oke[1] · David O. Adekunle[1] · Olufeyikemi A. Adeleke[2] · Omowumi T. Akinola[2] · Abiodun V. Emmanuel[3] · Oluwatoba E. Oyeneyin[3]

Abstract

Three new Schiff bases, (Z)-2-(4-(dimethylamino)benzylidene)-N-methylhydrazinecarbothioamide (PDM), (Z)-2-(2-hydroxy-5-nitrobenzylidene)-N-methylhydrazinecarbothioamide (5NS) and (Z)-2-(4-cyanobenzylidene)-N-methylhydrazinecarbothioamide (4CN) of thiosemicarbazone-benzaldehyde derivatives were synthesized by condensation reaction. These compounds were formed from the reaction of 4-methyl-3-thiosemicarbazide with p-dimethylaminobenzaldehyde, 5-nitrosalicylaldehyde and 4-formylbenzonitrile respectively. The molecules synthesized were screened against bacterial isolates; Gram-positive (*Staphylococcus aureus* and *Bacillus cereus*), and Gram-negative (*Klebsiella pnuemoniae* and *Pseudomonas aeruginosa*) bacteria using agar well diffusion technique, supported by molecular docking and theoretical analysis through computational approach adopting a coupled DFT-B$_3$LYP and 6-31G(d) basis set. The in-vitro antibacterial studies proofed that the compounds have a broad-spectrum antibacterial activity against the bacterial isolates while 5NS (21.0 mm) and PDMA (9.5 mm) have higher antibacterial activities than the standard drug, streptomycin against *Staphylococcus aureus* (16.5 mm) and *Pseudomonas aeruginosa* (9.0 mm) respectively. Theoretical studies and molecular docking established the fact that these Schiff bases could be explored further as bioactive compounds against bacterial infections and also as corrosion inhibitors of metals in the oil and gas industry.

✉ Adesoji A. Olanrewaju, adesoji.olanrewaju@bowen.edu.ng; sojylanrey2009@gmail.com | [1]Chemistry and Industrial Chemistry Programmes, College of Agriculture, Engineering and Science, Bowen University, Iwo, Nigeria. [2]Microbiology Programme, College of Agriculture, Engineering and Science, Bowen University, Iwo, Nigeria. [3]Theoretical and Computational Chemistry Unit, Department of Chemical Sciences, Adekunle Ajasin University, Akungba-Akoko, Nigeria.
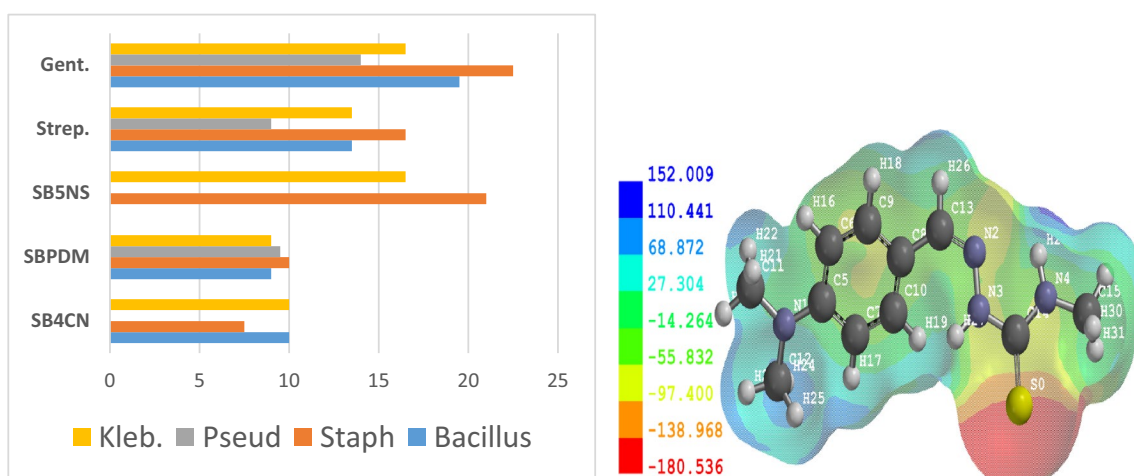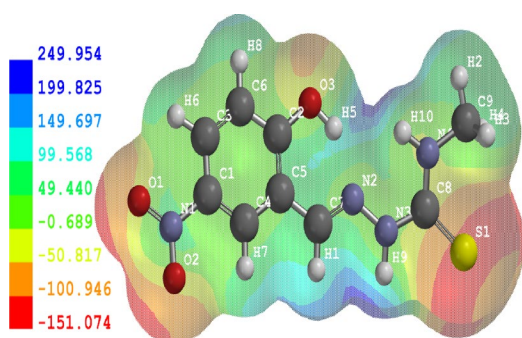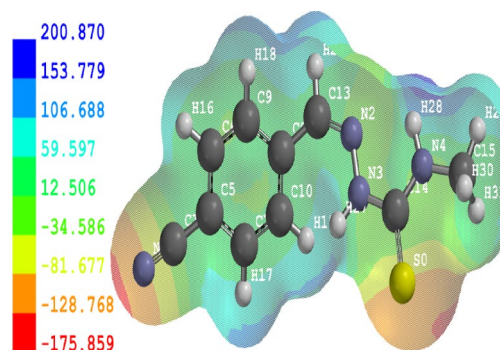
Graphical abstract

Histogram of the antibacterial activity of the Schiff bases & drugs

Electrostatic potential map of PDM

Electrostatic potential map of 5NS

Electrostatic potential map of 4CN

1 Introduction

Schiff bases (ScBs) are chemical mixtures or compounds with azomethine (–HC=N–) or an imine (>C=N–) functional group that are essential parts, which resemble aldehydes or ketones and are frequently employed as catalysts, pigments and dyes, as well as to stabilize polymers [1]. The aromatic aldehyde-based Schiff base molecules are more stable than that of the aliphatic aldehyde-based types, which in many occasions or cases are not even stable. The stability in the former is due to the presence of conjugation whereas the latter is vulnerable to free polymerization [2]. The major class of chemical compounds known as Schiff bases includes a variety of biologically diverse molecules [3–7]. The presence of donor atoms such as oxygen,

nitrogen or sulphur in these compounds enable them to possess wide range of biological applications and formation as a bidentate or tridentate chelate ligands enhancing their structural stability with metal ions/atoms or as a mixed ligand chelates [8–11].

Since the earliest days of the discovery of antibiotics, nature has been the main source of inspiration for the creation of novel antibiotics [12]. Meanwhile, antibiotic resistance has become an increasingly serious public danger in recent years due to its occurrence in hospitals, communities, and the environment. Antibiotic misuse has been linked to an increase in bacterial resistance, which has been linked to a decline in the effectiveness of the scarce medicines that are still accessible [13, 14]. Large doses of antibiotics used in human treatments, as well

as for farm animals and even fish in aquaculture, led to the selection of pathogenic bacteria resistant to various medications [15]. Multidrug resistance (MDR) is a kind of acquired resistance microorganisms show to one or more classes of antimicrobials and, on this base, they can be classified into: multidrug-resistant bacteria, extensively drug resistant (i.e., resistant to all but one or two classes) or pandrug-resistant (i.e., resistant to all available classes) [13, 14, 16, 17].

However, there is an urgent need for more efficient antibacterial and antifungal therapies because of the high mortality rates linked to diseases caused by bacteria and fungi as well as the rising quantity of multidrug-resistant strains in which Schiff bases may be taken into consideration. Thiosemicarbazones are a class of organic-based compounds that have been demonstrated to possess a variety of biological activities, such as antibacterial, antifungal, antiviral, and anticancer properties [18–21]. Earlier this decade, thiosemicarbazones have gained significant recognition as potential drug candidates due to their diverse pharmacological properties. The incorporation of benzaldehyde moiety into thiosemicarbazones has been reported to enhance their antimicrobial activities [22, 23]. Consequently, they are potential candidates for the development of new antimicrobial drugs.

In addition to the experimental antimicrobial and anticancer studies, computational methods and molecular docking have also been employed to investigate the potential activities of Schiff bases and their derivatives [24–26]. Herein, we also adopted the computational and molecular docking studies to find out the E_{HOMO} and E_{LUMO}, the global hardness (η) and the energy gap ($\Delta Egap$), Muliken charge distribution alongside Fukui function, electrostatic potential maps (EPM), Monte Carlo simulation for adsorption parameters of the adsorbed molecules on Fe(110) and molecular docking analysis using four different bacterial receptors: 6VBC, IVQQ, 4JVI and 4XVZ for the new synthesized thiosemicarbazone-benzaldehyde derivatives. Computational studies have the advantage of predicting the biological activity of compounds prior to their synthesis and characterization, thereby saving time and resources [27].

Therefore, this study, focuses on the synthesis, computational studies, in-vitro and in-silico antibacterial studies of selected thiosemicarbazone-benzaldehyde derivatives with the aim of exploiting their potent antibacterial activities as alternative antibiotics.

2 Experimental

2.1 Materials and reagents

AK Scientific, Central Drug House (CDH) Chemicals, Sigma-Aldrich, Loba Chemie, Moly Chem, and other well-known commercial organizations provided all of the analytical grade chemicals and solvents utilized, and they were all used immediately. The chemicals are 4-formylbenzonitrile 98% (GC) or 4-cyanobenzaldehyde, 2-hydroxy-5-nitrobenzaldehyde 95%, 4-dimethylamino benzaldehyde, 4-methyl-3-thiosemicarbazide 95%, streptomycin, gentamycin, posaconazole, Muller Hinton agar, absolute ethanol, Dimethylsulphoxide (DMSO). For the preparation of each concentration of all the compounds under research, DMSO solvent was utilized.

2.2 Preparation of the Schiff bases (SBs)

2.2.1 Preparation of the (Z)-2-(4-(dimethylamino) benzylidene)-N-methylhydrazinecarbothioamide (PDMA)

Drop by drop, 1.21×10^{-2} mol (1.27 g) of 4-methyl-3-thiosemicarbazide in absolute ethanol was added to a stirring solution of (1.80 g) 4-dimethylaminobenzaldehyde in approximately 40 milliliter of absolute ethanol. After adding 4–6 drops of acetic acid, the resulting yellowish-green solution was refluxed for 3–4 h. The yellowish-green product that developed after cooling to room temperature was filtered before being recrystallized from ethanol, dried, weighed and stored in a desiccator under anhydrous $CaCl_2$. The title compound's yield was 1.75 g (61%).

2.2.2 Preparation of the (Z)-2-(2-hydroxy-5-nitrobenzylidene)-N-methylhydrazinecarbothioamide (5NS)

To a stirring solution of 1.08×10^{-2} mol (1.80 g) of 2-hydroxy-5-nitrobenzaldehyde in 20 mL of absolute ethanol, 1.08×10^{-2} mol (1.26 g) of 4-methyl-3-thiosemicarbazide in 15 mL of absolute ethanol was added drop wise. Following the addition of 0.1–0.2 mL drops of acetic acid, the resulting yellow-colored solution was refluxed for 3–4 h. Following filtering, ethanol was recrystallized from the yellow product that formed after cooling to room temperature. 2.45 g (89%) of the product in the title was produced.

2.2.3 Preparation of the (Z)-2-(4-cyanobenzylidene)-N-methylhydrazinecarbothioamide (4CN)

Dropwise addition of 1.37×10^{-2} mol (1.44 g) of 4-methyl-3-thiosemicarbazide in 15 mL of absolute ethanol was made to a stirring solution of 1.37×10^{-2} mol (1.80 g) of 4-cyanobenzaldehyde in 20 mL of absolute ethanol. The resulting creamy-white solution was refluxed for 3–4 h after 0.1–0.2 mL drops of acetic acid were added. The creamy-white product generated after cooling to room temperature was filtered, and ethanol was recrystallized from it. The product in the title was manufactured in 2.89 g (96%) total.

2.3 Antimicrobial studies

All the compounds were screened for their in-vitro antibacterial activity using agar diffusion method.

2.3.1 In-vitro antibacterial assay

The antibacterial activity of the prepared ligands was determined by the agar well diffusion method [28]. The Schiff base (SB) compounds were studied against bacterial isolates obtained from Microbiology Programme of Bowen University, Iwo, Nigeria. Two Gram-positive (Staphylococcus aureus and Bacillus sp (cereus)) and two Gram-negative (Klebsiella pnuemoniae and Pseudomonas sp (aeruginosa)) bacteria were used as test subjects for the compounds. The tested bacterial isolates were grown again over night on Nutrient agar plates to obtain 24 h old culture. The turbidity of the broth was changed to 0.5 McFarland, or 1.5 108 CFU. Then, using a swab stick, each bacterial culture was inoculated by sweeping the swab across the entire Muller Hinton agar surface. In order to achieve a uniform dispersion of the inoculums, this technique was repeated by streaking twice more while rotating the plate. After some minutes, agar well was punched on the surface of inoculated agar plates using sterile 7 mm Cork borer, thereafter 10 µg of the SB compound was filled into the well using sterile micro pipette. The plates were incubated at 37 °C for 24 h after standing at room temperature for 30 min to allow the SB component to diffuse into the agar well. Following incubation, the diameter of the inhibition zone was measured to the nearest millimeter (mm), and all the plates were checked for the presence of bacterial growth inhibition. The test was performed in duplicate while the mean value was recorded. Standard antibiotic Streptomycin (10 µg) and Gentamicin (10 µg) served as the positive control, while DMSO served as a negative control or blank. Presentation of the result is shown in Table 1.

## 2.4 Computational studies

2.4.1 DFT optimization and Monte Carlo simulation

The Schiff bases (PDMA, 5NS and 4CN) were modeled and subjected to conformation search to obtain the most stable conformers (lowest energy configuration) using molecular mechanics force field before full optimization with a hybrid DFT (B3LYP) and 6-31G(d) basis set [29, 30], on Spartan 14 software [31]. The level of the theory was chosen because of its consistence with experimental findings [32, 33]. The molecular descriptors like the frontier molecular orbitals energies (E_{HOMO} and E_{LUMO}), energy band gap, ionization potential, electron affinity, hardness, softness, electrophilicity, fraction of electrons transferred and electron backdonation were obtained from the optimization. These descriptors will provode information about the behaviour of the molecules [34]. The Fukui indices were calculated to ascertain the sites for nucleophilic and electrophilic attacks, according to the method described earlier [35]. The molecules were also investigated for their corrosion inhibitive potentials on Fe(110) using Forcite and adsorption locator tools on Material Studio to obtain the adsorption parameters, as described earlier [29, 34, 36].

Table 1 Antibacterial activities of the Schiff bases and the standard drugs (mm)

| Compounds/bacteria	Bacillus cereus	Staphylococus aureus	Pseudomona aeruginosa	Klebsiella pneumonia
4CN	10.0 ± 0	7.5 ± 0.71	R	10.0 ± 0
PDMA	9.0 ± 1.41	10.0 ± 0	9.5 ± 0.71	9.0 ± 1.41
5NS	R	21.0 ± 1.41	R	16.5 ± 0.71
Streptomycin (+ve)	13.5 ± 2.12	16.5 ± 0.71	9.0 ± 1.41	13.5 ± 2.12
Gentamycin (+ve)	19.5 ± 3.54	22.5 ± 3.54	14.0 ± 1.41	16.5 ± 0.71
DMSO (−ve)	R	R	R	R

Mean zone of inhibition (mm) of the values were presented with standard deviation, while streptomycin and gentamycin were the positive reference standard and DMSO as a negative control
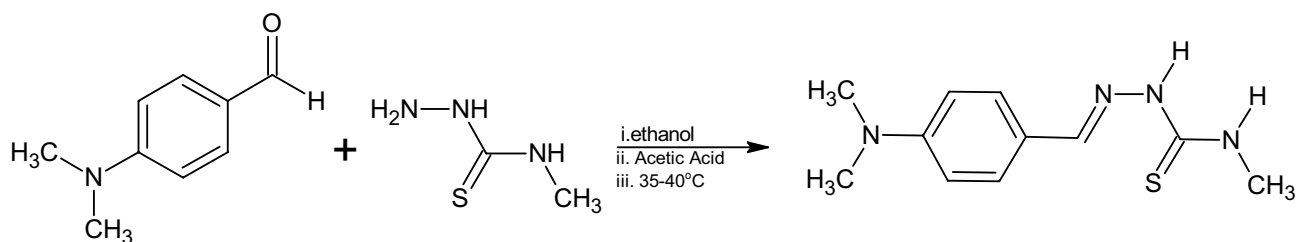
Scheme 1 Synthesis of (Z)-2-(4-(dimethylamino)benzylidene)-N-methylhydrazine carbothioamide (PDMA)
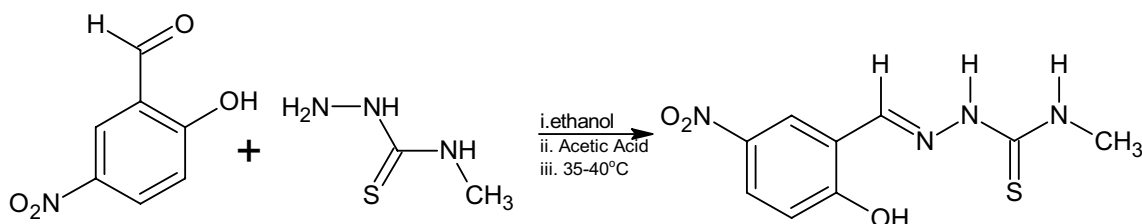
Scheme 2 Synthesis of (Z)-2-(2-hydroxy-5-nitrobenzylidene)-N-methylhydrazine carbothioamide (5NS)
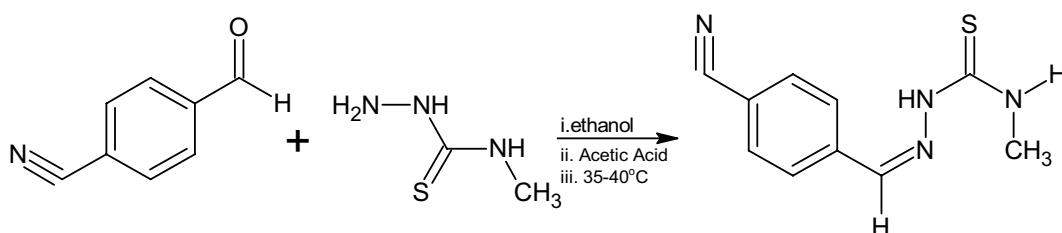
Scheme 3 Synthesis of(Z)-2-(4-cyanobenzylidene)-N-methylhydrazinecarbothioamide (4CN)

2.4.2 Molecular docking method

A penicillin-binding protein 2 (PBP-2) with pdb ID: 6VBC (resolution 1.55 Å), Bacillus cereus was employed as a receptor for PBP2's transpeptidase domain, which was isolated from the cephalosporin-resistant strain H041 of *N. gonorrhoeae*. A penicillin Binding Protein 2 A (PBP-2 A) with pdb ID: 1VQQ (resolution 1.80 Å) was used for Staphylococcus aureus. Pseudomonas species. A transcriptional regulator MvfR with pdb ID: 4JVI (resolution 2.9 Å) was used for Pseudomonas species. A beta lactamase receptor with pdb ID: 4XUZ (resolution 1.5 Å) was used for Klebsiella species. The molecules and standard drugs (streptomycin and gentamycin) were docked at the active sites (x = − 6.06, y = 5.02, z = 22.32 for 6VBC), (x = 17.47, y = 28.49, z = 38.90 for 1VQQ), (x = − 32.45, y = 56.43, z = 7.62 for 4JVI) and (x = 53.9, y = 39.12, z = 10.38 for 4XUZ), as generated by sitemap, all on Maestro/Schrodinger suit [37–39].

3 Results and discussion

3.1 Schematic formation of the Schiff bases

The reaction scheme of each Schiff bases formation (PDMA, 5NS and 4CN) from their starting materials and reaction conditions were shown below:

3.2 In-vitro antibacterial studies

In Table 1, the mean value of the synthetic compounds' antibacterial activity was noted. A standard medication/drug was used to compare the zone of inhibition, which was measured in millimeters. The findings demonstrate that these synthesised compounds (Scheme 1, 2, 3) were active to varied degrees in preventing the growth of the bacteria *Staphylococcus aureus*, *Bacillus cereus*, *Klebsiella pnuemoniae*, and *Pseudomonas aeruginosa*, which ranged in size from 7.5 to 22.5 mm as shown in figure 1. In general, all of

Fig. 1 Histogram representation of the antibacterialactivity of the compounds and the drugs
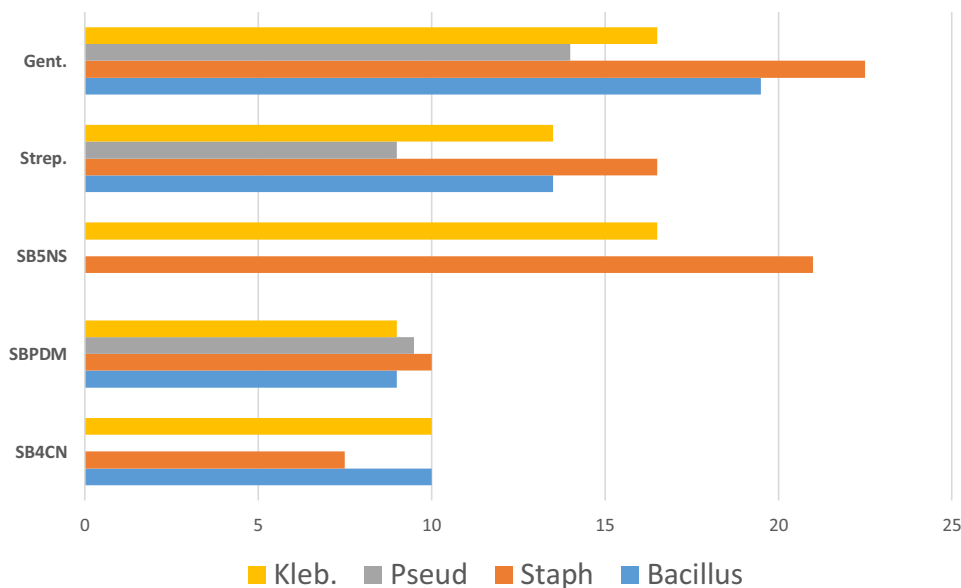
the substances were extremely effective against Klebsiella pneumonia and Staphylococcus aureus but out of the three compounds or ligands, 5NS showed the highest inhibition to *Staphylococcus aureus and Klebsiella pneumonia* with 21.0 mm and 16.5 mm respectively. In comparison to the standard drugs, it was reveal that against *Staphylococcus aureus*, gentamycin (22.5 mm) has little higher inhibition of 1.5 mm disparity to 5NS Schiff base (21.0 mm), while the latter exhibit a very high activity than streptomycin (16.5 mm). Interestingly, both gentamycin and 5NS has the same inhibition against *Klebsiella pneumonia*. Several authors have worked on different types of Schiff bases and have concluded that the presence of imine groups, hydroxyl groups, and nitrogen groups that form part of Schiff bases' components have the ability to form hydrogen bonding connections with cellular compartments of the bacteria, which may then result in their antibacterial activity [40]. In a way of contrast, 5NS showed no activity against *Bacillus cereus and Pseudomonas aeruginosa*. Antibiotic resistance in *Pseudomonas aeruginosa* has been documented, and the formation of efflux pumps present in this bacterium may prevent a drug from passing through their lipid membrane [41]. However, 4CN and PDMA showed activity against *Bacillus cereus* but not as more active as that of the standard drugs. Interestingly, PDMA (9.5 mm) reveal higher activity of inhibition than the streptomycin drug (9.0 mm) against

pseudomona auruginosa, although, less than gentamycin drug (14.0 mm) (Table 1).

The following is a list of the compounds' activity against each strain of bacterium in ascending order:

Bacilluscereus	: 5NS < PDMA < 4CN < Streptomycin< Gentamycin
Staphylococus aureus	: 4CN < PDMA < Streptomycin < 5NS <Gentamycin
Pseudomona aeruginosa	:4CN = 5NS < streptomycin < PDMA < Gentamycin
Klebsiella pneumonia	: PDMA < 4CN < Streptomycin < Gentamycin= 5NS

In comparison to PDM and 4CN, the findings showed that 5NS Schiff base exhibited the strongest antibacterial activity and even very close and same activity with the standard drugs against some antibacterial strains.

3.3 DFT results

The E_{HOMO} and E_{LUMO} of the compounds (Table 2) revealed that PDMA has the highest HOMO energy value (-5.16 eV), an indication that it has the highest ability to donate electrons, the E_{HOMO} trend follows PDMA > 4CN > 5NS. High E_{HOMO} of compound PDMA indicates that it possesses a

Table 2 Electronic properties and reactivity descriptors of the compounds

Compounds	E_{HOMO} (eV)	E_{LUMO} (eV)	I (eV)	A (eV)	E_g (eV)	η (eV)	δ (eV^{-1})	χ (eV)	ω (eV)
PDMA	-5.16	-1.10	5.16	1.10	4.06	2.03	0.49	3.13	2.41
5NS	-6.07	-2.47	6.07	2.47	3.60	1.80	0.56	4.27	5.06
4CN	-5.87	-2.40	5.87	2.40	3.47	1.735	0.58	4.14	4.97

large potency of electrons' donation to the metal atom with low-lying unfilled d-orbital and another molecule. Low LUMO value is required for effective electron-withdrawal in a molecule from the orbitals of another molecule or biological cell. 5NS showed the highest stabilized LUMO (− 2.47 eV), showing that it has the highest capacity to receive electrons. The LUMO energy follows the order PDMA > 4CN > 5NS. A direct consequence of the E_{HOMO} and E_{LUMO} (being negative of each other), are the ionization

potential (I) and electron affinity (A) respectively [29, 35]. High HOMO value indicates low ionization potential (ease of donating electron) while low LUMO indicates high electron affinity (ease of accepting electrons). The substitution of dimethylamine in PDMA and cyanide in 4CN on the parent structure compared to electron-withdrawing nitro group in 5NS significantly lowered their ionization potentials while the nitro group in 5NS stabilized its LUMO

Table 3 Charges of Mulliken and Fukui indices of PDMA

PDMA	qk (N + 1)	qk (N)	qk (N − 1)	fk+	fk−	Δfk
S0	− 0.477	− 0.332	− 0.111	− 0.145	− 0.221	0.076
N1	− 0.445	− 0.472	− 0.443	0.027	− 0.029	0.056
N2	− 0.375	− 0.256	− 0.221	− 0.119	− 0.035	− 0.084
N3	− 0.427	− 0.453	− 0.397	0.026	− 0.056	0.082
N4	− 0.571	− 0.563	− 0.554	− 0.008	− 0.009	0.001
C5	0.195	0.375	0.387	− 0.18	− 0.012	− 0.168
C6	− 0.153	− 0.193	− 0.167	0.04	− 0.026	0.066
C7	− 0.159	− 0.194	− 0.165	0.035	− 0.029	0.064
C8	0.189	0.144	0.17	**0.045**	− 0.026	**0.071**
C9	− 0.221	− 0.19	− 0.171	− 0.031	− 0.019	− 0.012
C10	− 0.258	− 0.218	− 0.201	− 0.04	− 0.017	− 0.023
C11	− 0.275	− 0.315	− 0.345	0.04	0.03	0.01
C12	− 0.276	− 0.316	− 0.344	0.04	**0.03**	**0.012**
C13	− 0.107	− 0.028	− 0.018	− 0.079	− 0.01	− 0.069
C14	0.37	0.382	0.366	− 0.012	0.016	− 0.028
C15	− 0.275	− 0.288	− 0.31	0.013	0.022	− 0.009

The bold values are the most active sites (electrophilic and nucleophilic) for the molecules, as captured in sect. 3.4

Table 4 Mulliken charges and Fukui indices of 5NS

5NS	qk (N + 1)	qk (N)	qk (N − 1)	fk+	fk−	Δfk
S1	− 0.432	− 0.282	0.071	− 0.15	− 0.353	0.203
N1	0.316	0.377	0.401	− 0.061	− 0.024	− 0.037
O1	− 0.474	− 0.398	− 0.358	− 0.076	− 0.04	− 0.036
O2	− 0.487	− 0.403	− 0.372	− 0.084	− 0.031	− 0.053
O3	− 0.698	− 0.646	− 0.592	− 0.052	− 0.054	0.002
C1	0.284	0.273	0.275	0.011	− 0.002	0.013
C2	0.273	0.321	0.35	− 0.048	− 0.029	− 0.019
C3	− 0.208	− 0.149	− 0.12	− 0.059	− 0.029	− 0.03
C4	− 0.258	− 0.239	− 0.211	− 0.019	− 0.028	0.009
C5	0.111	0.092	0.088	**0.019**	0.004	**0.015**
C6	− 0.179	− 0.171	− 0.158	− 0.008	− 0.013	0.005
C7	0.023	0.094	0.119	− 0.071	− 0.025	− 0.046
N2	− 0.417	− 0.344	− 0.342	− 0.073	− 0.002	− 0.071
N3	− 0.429	− 0.443	− 0.28	0.014	− 0.163	0.177
N4	− 0.574	− 0.569	− 0.546	− 0.005	− 0.023	0.018
C8	0.379	0.383	0.358	− 0.004	0.025	− 0.029
C9	− 0.277	− 0.294	− 0.324	0.017	**0.03**	**-0.013**

The bold values are the most active sites (electrophilic and nucleophilic) for the molecules, as captured in sect. 3.4

orbitals and is responsible for the electron withdrawing potential.

The global hardness (η) and the energy gap (ΔEgap) of the compounds are in the same order as they are directly related [29, 35]. Compounds with low ΔEgap and η are very reactive and unstable. 4CN has the lowest band gap (3.47 eV), followed by 5NS (3.60 eV) and PDMA (4.06 eV), in the same manner with their hardness values 4CN (1.735

Table 5 Mulliken charges and Fukui indices of 4CN

4CN	qk (N + 1)	qk (N)	qk (N-1)	fk+	fk-	Δfk
S0	− 0.441	− 0.296	0.09	− 0.145	− 0.386	0.241
C1	0.171	0.243	0.273	− 0.072	− 0.03	− 0.042
N1	− 0.56	− 0.469	− 0.415	− 0.091	− 0.054	− 0.037
N2	− 0.356	− 0.227	− 0.226	− 0.129	− 0.001	− 0.128
N3	− 0.437	− 0.45	− 0.391	0.013	− 0.059	0.072
N4	− 0.569	− 0.562	− 0.54	− 0.007	− 0.022	0.015
C5	0.085	0.131	0.153	− 0.046	− 0.022	− 0.024
C6	− 0.151	− 0.134	− 0.122	− 0.017	− 0.012	− 0.005
C7	− 0.147	− 0.134	− 0.12	− 0.013	− 0.014	0.001
C8	0.177	0.156	0.151	**0.021**	0.005	**0.016**
C9	− 0.207	− 0.183	− 0.164	− 0.024	− 0.019	− 0.005
C10	− 0.242	− 0.213	− 0.2	− 0.029	− 0.013	− 0.016
C13	− 0.083	− 0.034	0.019	− 0.049	− 0.053	0.004
C14	0.377	0.381	0.358	− 0.004	0.023	− 0.027
C15	− 0.275	− 0.292	− 0.325	0.017	**0.033**	− 0.016

The bold values are the most active sites (electrophilic and nucleophilic) for the molecules, as captured in sect. 3.4

Optimized molecule   **HOMO**   **LUMO of PDMA**
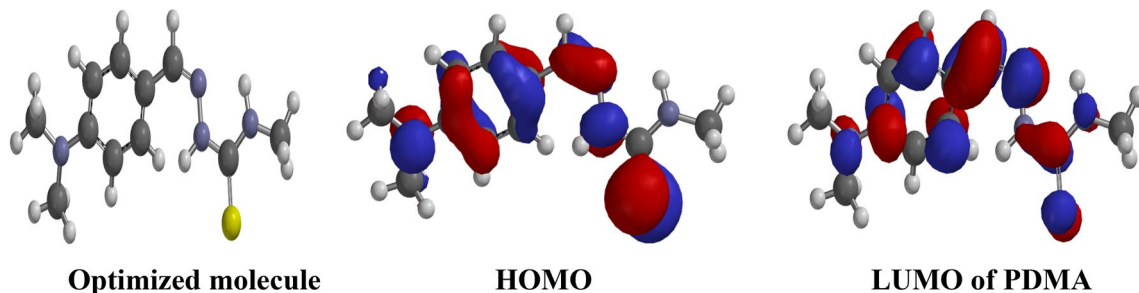
Fig. 2 Optimized molecule HOMO LUMO of PDMA

Fig. 3 Electrostatic potential map of PDMA
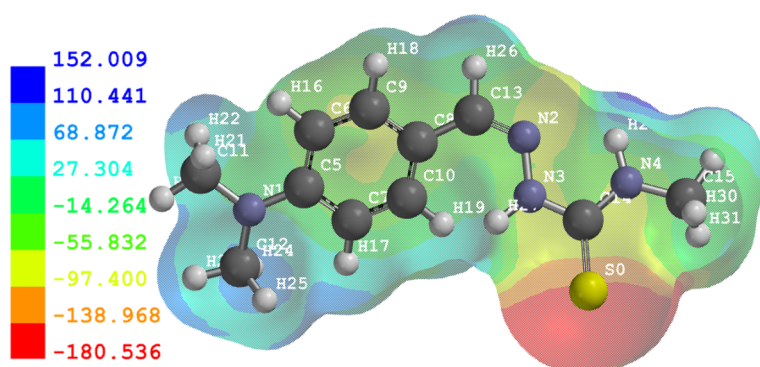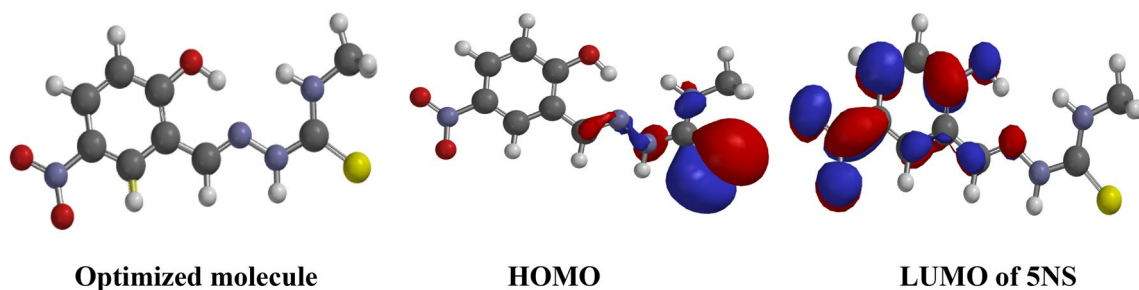
Fig. 4 Optimized molecule HOMO LUMO of 5NS

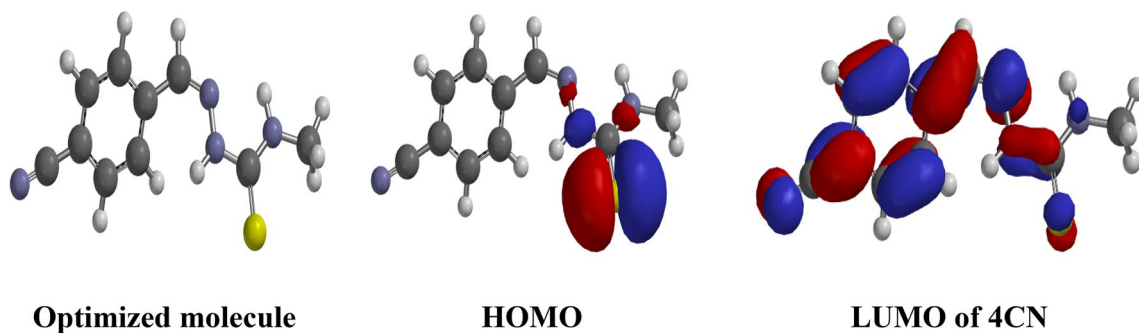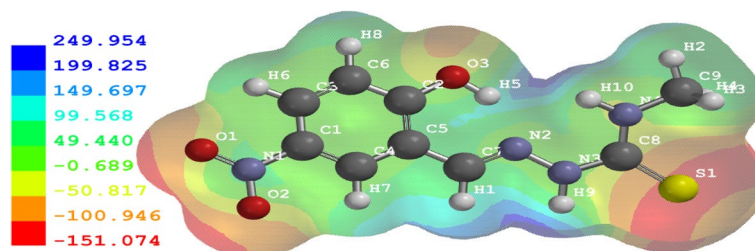**Fig. 5** Electrostatic potential map of 5NS

Fig. 6 Optimized molecule HOMO LUMO of 4CN

eV), followed by 5NS (1.80 eV) and PDMA (2.03 eV). The chemical reactivity, as deduced from the chemical softness (δ) will increase in the order: 4CN (0.58 eV^{-1}) > 5NS (0.56 eV^{-1}) > PDMA (0.49 eV^{-1}). The values of ΔEgap, η and δ here are similar with those in literature for materials used as corrosion inhibitors or as potential drug candidates [42, 43]. The direction of flow of electron between the metal surface and the inhibitor is specified by the electronegativity (χ) untill a balance in chemical potential is achieved while global electrophilicity (ω) determines energy stabilization between it and either the metal surface or a biological target. The electronegativity follows the order: 5NS (4.27 eV) > 4CN (4.14 eV) > PDMA (3.13 eV), the electrophilicity follows the same order: 5NS (5.06 eV) > 4CN (4.97 eV) > PDMA (2.41 eV). This shows that 5NS is the most electrophilic and more reactive than 4CN and PDMA. 5NS, among others, will be the most promising drug candidate [43]. On the adsorption of the molecules on the surface of the metal, most importantly iron (with electronegativity value of 7 eV), the higher electronegativity type receives electrons from the type with lower electronegativity value. The molecules have lesser electronegativities (χ = 3.13–4.27 eV) than iron's, suggesting that they have capacity to transfer electron to the surface of the metal.

3.4 Mulliken charge distribution in conjunction with Fukui functions

Compounds' potential reactive site can be inferred from the Mulliken charge distribution on those compounds. Tables 3, 4, and 5 display a few charges of Mulliken that

Table 6 Adsorption parameters of the adsorbed molecules on Fe(110) [all energies are in kcal/mol]

System	E_{Tot}	E_{Ads}	E_{Rigid}	E_{Def}
Fe(110)-PDMA	−13127.4	−17007.4	13355.7	−3650.0
Fe(110)-5NS	−44262.9	−82859.6	−45118.5	−3774.1
Fe(110)-4CN	−43507.9	−82092.5	−44242.9	−3784.9

were computed for the compounds' anionic, cationic, and neutral categories. Atoms with $\Delta fk > 0$ are nucleophiles whereas those with $\Delta fk < 0$ are electrophiles. Considering Table 3, the C8 on PDMA has the highest f_k^+ (0.045) with Δf_k (0.071) as the positive value, showing the nucleophilic attack's preferred position or region. The C12 atom has the maximum value of fk-, which is attained at a value of (0.03), and it prefers to attack other molecules there by electrophilically (at a value of Δf_k (−0.012)). From Table 4, the C5 atom of 5NS has the highest (0.019) and Δf_k (0.015) positive value showing the nucleophilic attack's preferred location. The C9 atom revealed the maximum value of f_k^- with value (0.03) and the Δf_k (−0.013) as negative value being its electrophilic attack's preferred site. Considering Table 5, the C8 atom of 4CN showed the maximum f_k^+ (0.021) and Δf_k (0.016)

positive value, establishing the nucleophilic attack's preferred site. The highest value of is obtained at C15 atom with value (0.033) has the maximum value of f_k^- and Δf_k (−0.016) negative value, insinuating to be its electrophilic attack's preferred site.

3.5 HOMO, LUMO and electrostatic potential maps

The optimized structure and reactive site maps of the molecules are displayed in Figs. 2, 3, 4, 5, 6, and 7. The HOMO of PDMA spreads across the benzylidene)-N-methylhydrazine and the sulphur atom, leaving out the methyl groups on the dimethylamino part and the amide group (Fig. 2) while its LUMO map also spread across the same area, including the nitrogen atom on the amide. The electrostatic potential map (EPM) reveals atoms that are electron rich or deficient. The EPM of PDMA (Fig. 3) indicates that the hydrazine nitrogen and sulphur atoms are the sites for electrophilic attack (red, orange) while the dimethylamino, benzylidene hydrogen atoms and amide hydrogen atoms are sites for nucleophilic attack (blue, green). The HOMO of 5NS spreads across the entire N-methylhydrazinecarbothioamide region starting from the imine group, leaving out the methyl groups on the amide group (Fig. 4) while its LUMO map spreads across

Fig. 7 Electrostatic potential map of 4CN
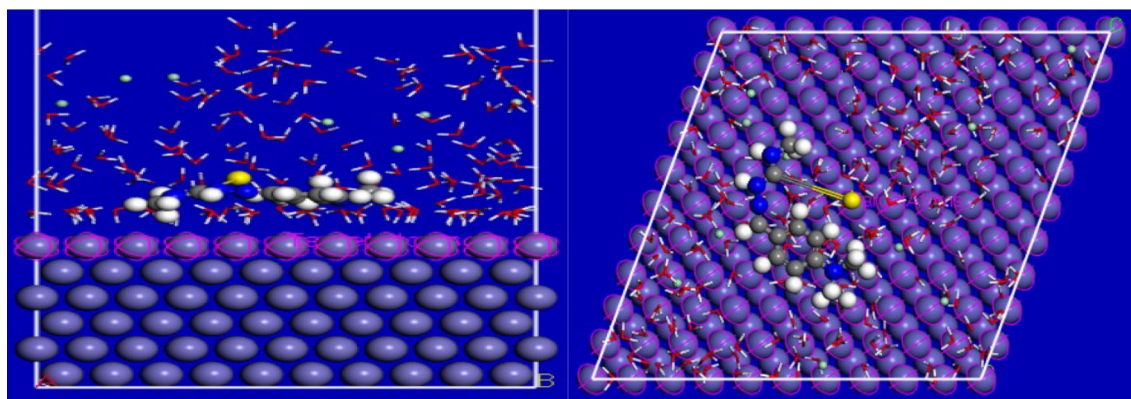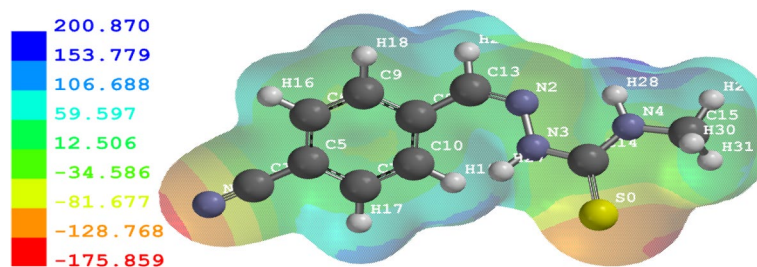
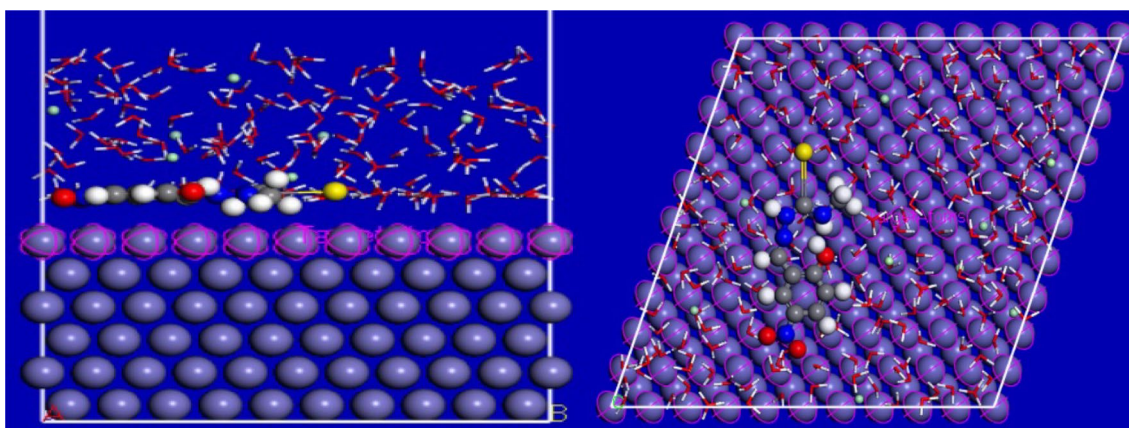**Fig. 8** Simulation of adsorption (side view and topview) of PDMA on Fe(110) surface

Fig. 9 Simulation of adsorption (side viewand top view) of 5NS on Fe(110) surface

Table 7 Binding affinities of the docked molecules and standard drugs (streptomycin and gentamycin) with different bacterial receptors

Molecules	Binding affinity (kcal/mol) for 6VBC	Binding affinity (kcal/mol) for 1VQQ	Binding affinity (kcal/mol) for 4JVI	Binding affinity (kcal/mol) for 4XUZ
PDMA	−4.629	−5.115	−6.464	−5.028
5NS	−4.810	−5.183	−5.895	−4.778
4CN	−4.243	−5.063	−6.382	−4.691
Streptomycin	−5.904	−5.474	−5.229	−3.988
Gentamycin	−3.996	−5.451	−7.069	−4.148
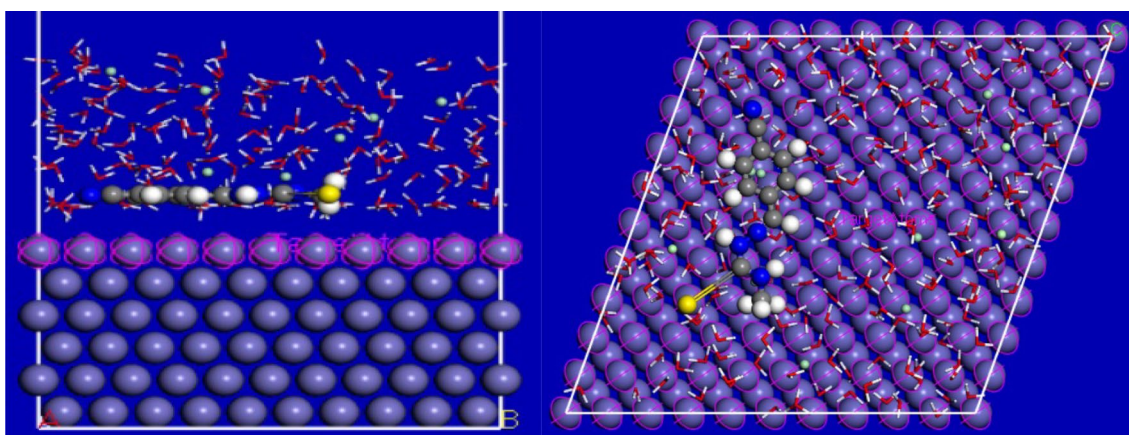
Fig. 10 Simulation of adsorption (side viewand top view) of 4CN on Fe(110) surface

the entire 2-hydroxy-5-nitrobenzylidene region, including the imime carbon and nitrogen. The EPM of 5NS (Fig. 5) indicates that the hydrazine nitro oxygen atoms, hydroxyl oxygen and sulphur atom are the sites for electrophilic attack (red, orange) while the benzylidene carbon and hydrogen atoms, imine goup, amide atoms (except the sulphur atom) are sites for nucleophilic attack (blue, green). The HOMO of 4CN is focused on the hydrazinecarbothio

area, with the sulphur atom being the most prominent (Fig. 6) while its LUMO map spreads across the same region as the HOMO, adding the entire 4-cyanobenzylidene part. The EPM of 4CN (Fig. 7) indicates that the cyano nitrogen and sulphur atom are the major sites for electrophilic attack (red, orange) while the other parts of the molecule are sites for nucleophilic attack (blue, green).
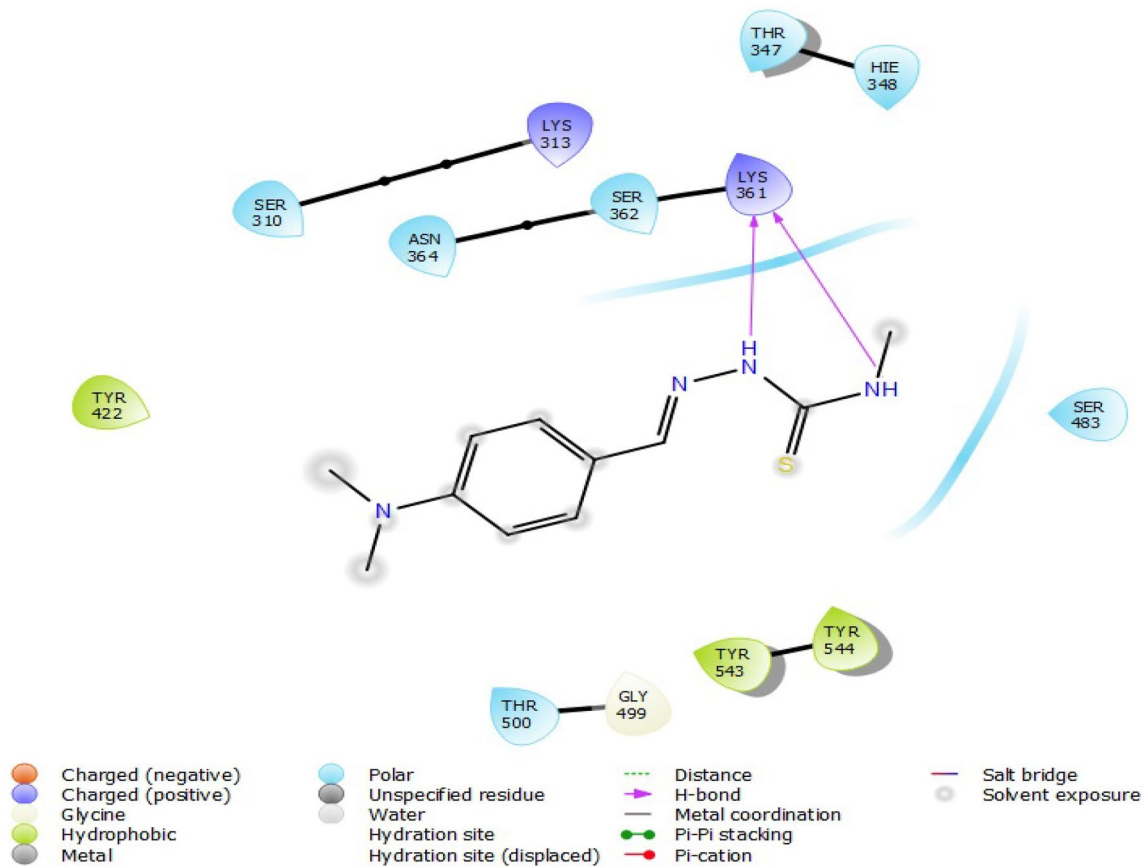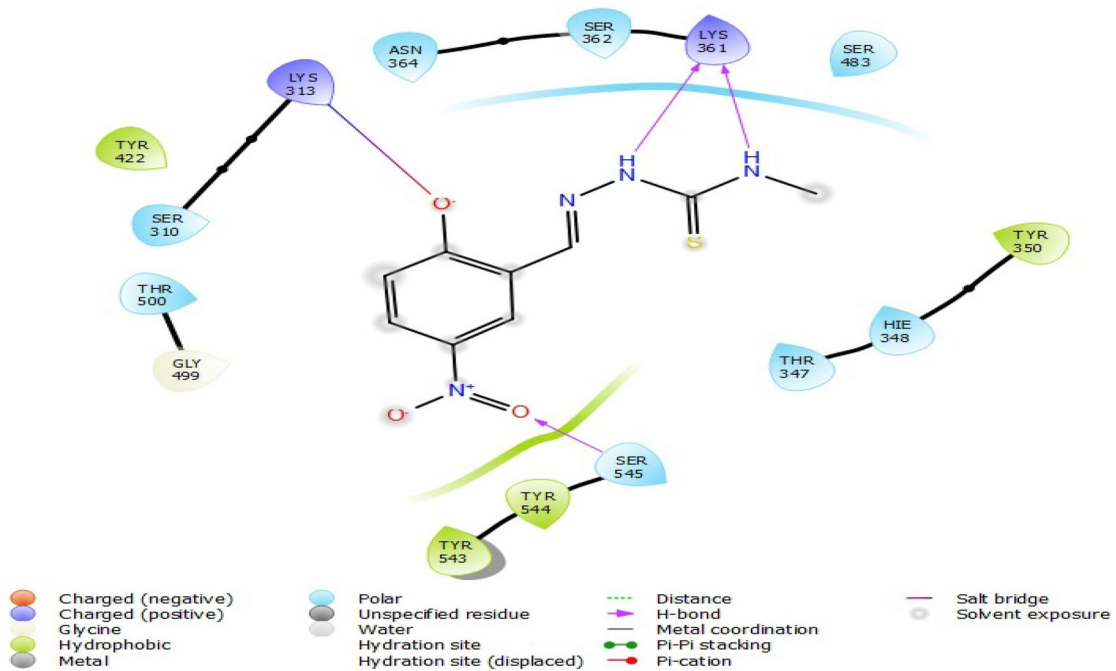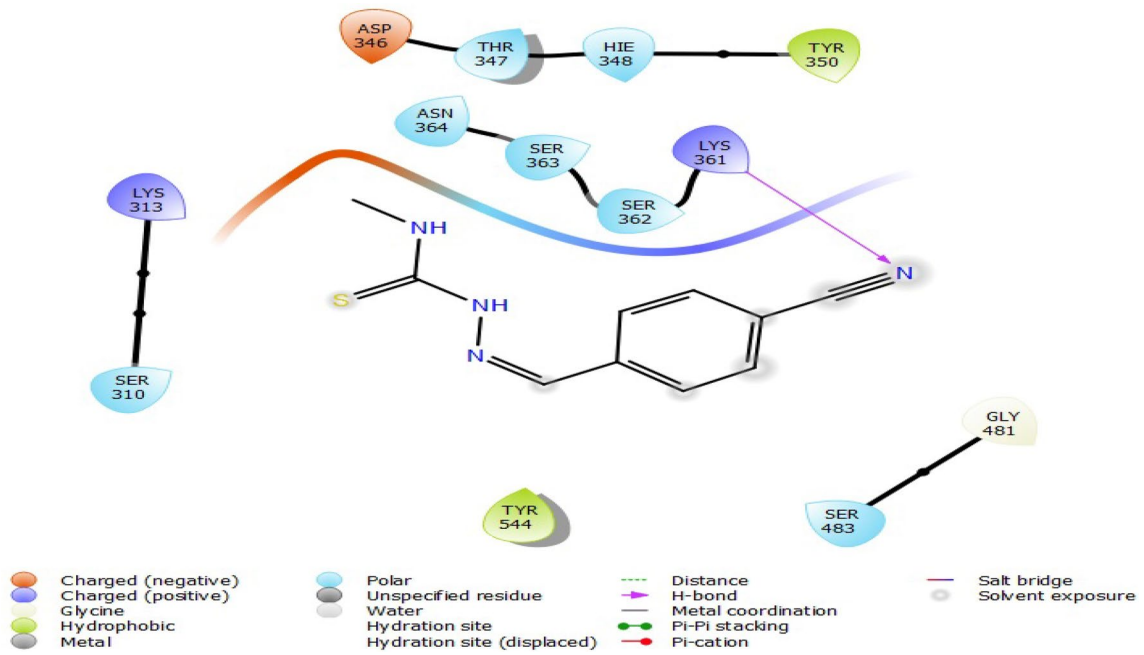
Fig. 11 PDMA with 6VBC

Fig. 12 5NS with 6VBC
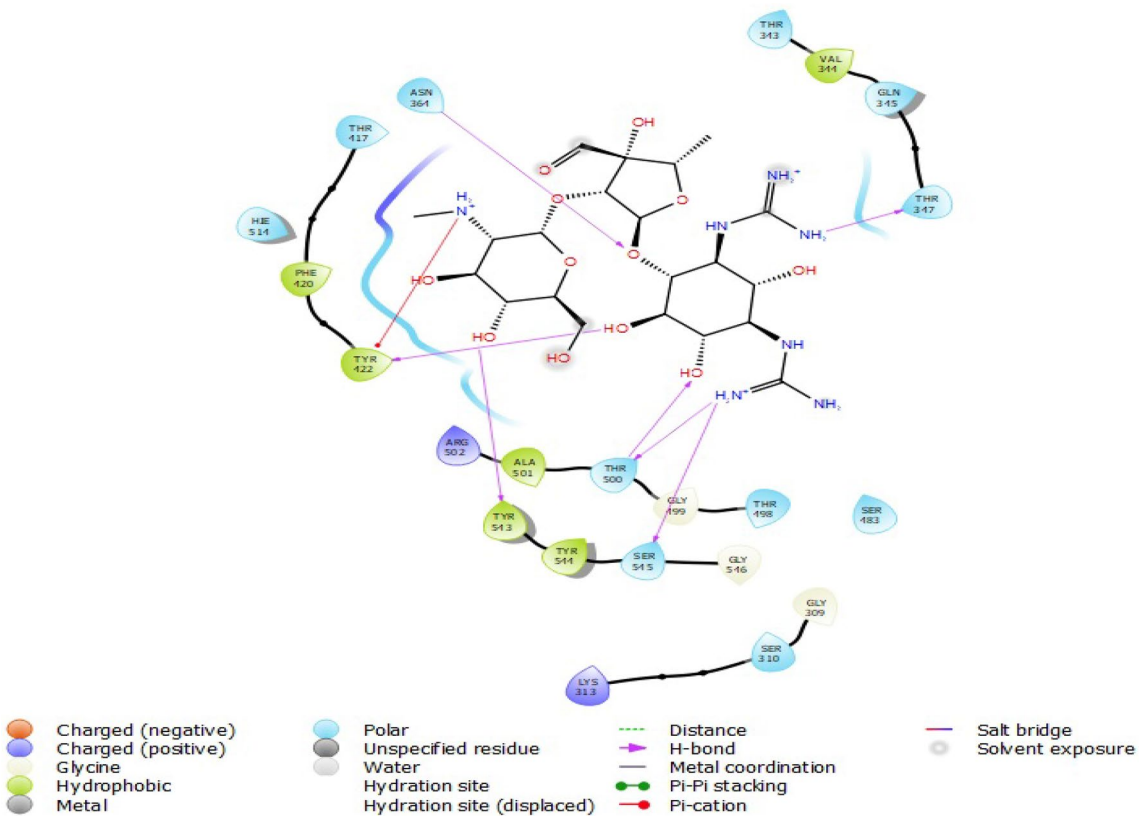
Fig. 13 4CN with 6VBC

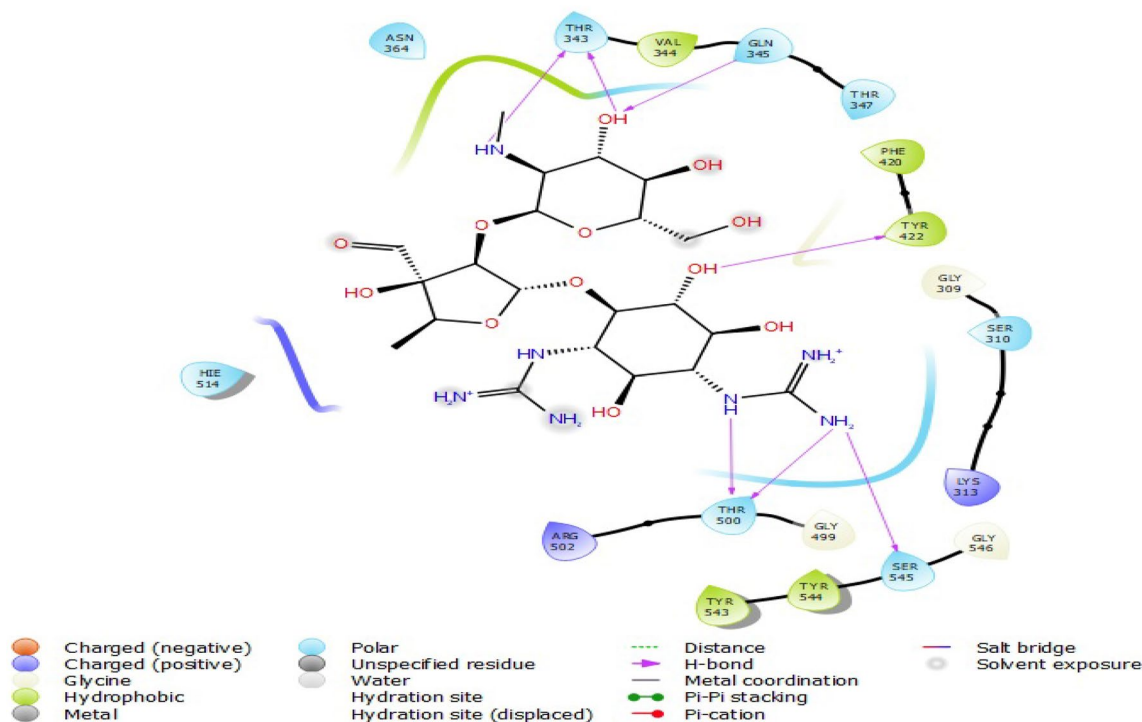

Fig. 14 Streptomycin with 6VBC

Fig. 15 Gentamycin with 6VBC

3.6 Monte Carlo simulation

The total energy of the iron-inhibitor (ETOT), energy of adsorption (EAds), energy of rigid adsorption (ERigid), and energy of deformation (EDef) of the Fe(110)-thiosemicarbazone-benzaldehyde complexes are provided in Table 6 based on the findings of the adsorption locator. Complexes' stability is correlated with their total energy (ETOT). The total energy takes the order: Fe(110)-5NS < Fe(110)-4CN < Fe(110)-PDMA, indicating that 5NS is the most thermodynamically stable of all the molecules on the surface of Fe(110). This further buttressed the DFT results. In addition, significant corrosion inhibitor adsorption on the surface of the metal has been linked to low E_{Ads}, the order of the E_{Ads} is Fe(110)-5NS < Fe(110)-4CN < Fe(110)-PDMA.

Figures 8, 9 and 10 reveal the side and top captions of the absorbed molecules on Fe(110) surface in aqueous solution. It's interesting to note that all of the inhibitors display a roughly side-by-side configuration to the iron plane in the MC simulation pictures, sufficient surface coverage, and significant water molecule displacement. The parallel arrangement of the inhibitors on the surface of the iron raises the possibility that the molecules could engage in reverse donation to the low-lying d-orbitals of

the Fe(110), interact with the metal surface via covalent and non-bonded interactions, and isolate the iron from the corrosive environment. Hence, they could be used as corrosion inhibitors, subject to gravimetric and electrochemical experiments conformation [29, 35, 44].

3.7 Molecular docking analysis

The docking scores of the molecules and standard drugs (streptomycin and gentamycin) are recorded on Table 7. For the PBP-2 transpeptidase receptor, 6VBC for *B. cereus*, PDMA has a binding affinity of − 4.629 kcal/mol with interaction between it and the amino acid residues of the receptor at LYS361 from the hydrogen atoms on the hydrazine and amide groups via hydrogen bonding (Fig. 11), 5NS has a docking score of -4.810 kcal/mol and interacted with the amino acid residues at LYS361 via the hydrogen atoms on the hydrazine and amide groups (hydrogen bonding), SER545 via the nitro oxygen (hydrogen bonding) and LYS313 from its hydroxyl oxygen via salt bridge (Fig. 12). 4CN has a docking score of − 4.243 kcal/mol with interactions at LYS361 through its cyano nitrogen via hydrogen bonding (Fig. 13). Streptomycin has a docking score with the 6VBC (− 5.904 kcal/mol) while interacting
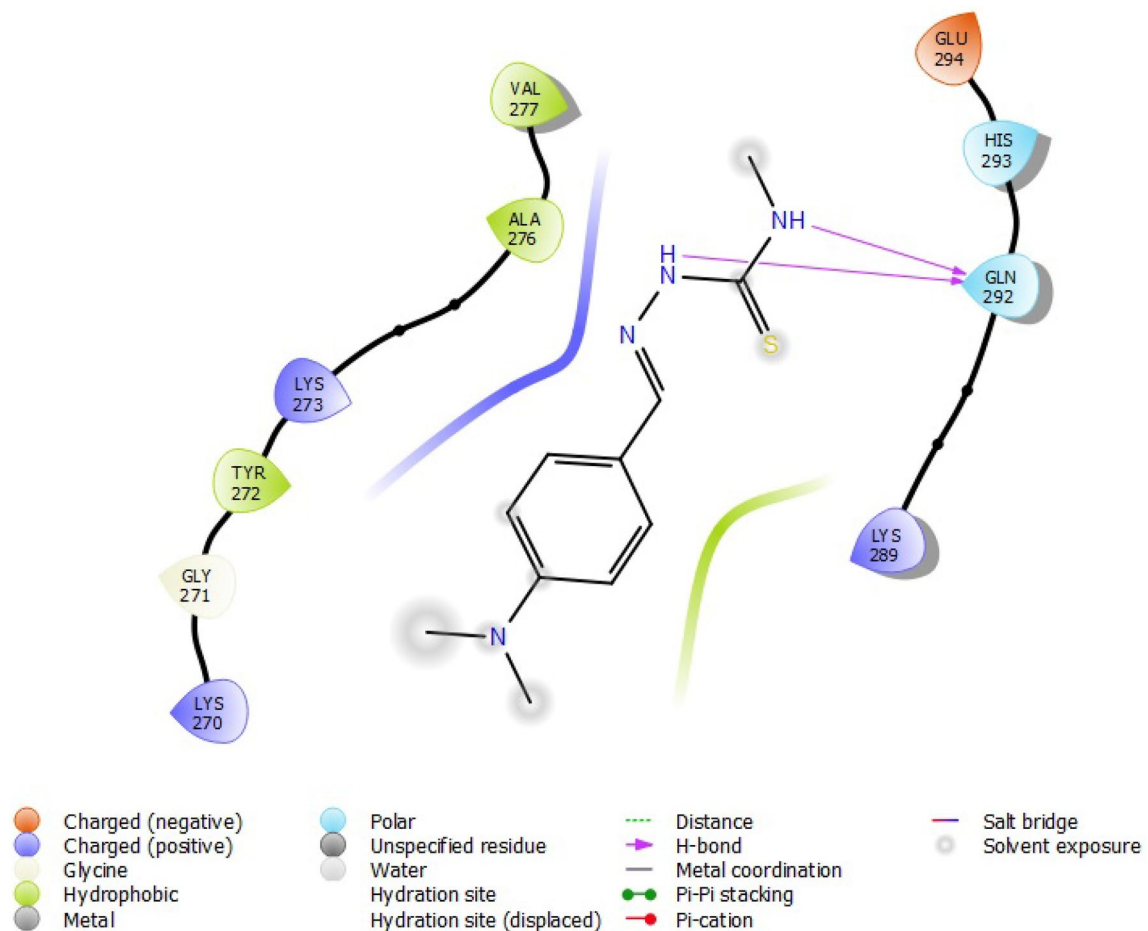
Fig. 16 PDMA with 1VQQ

through its oxygen atoms with ASN261, TYR422, TYR543, THR500, ASN364 via hydrogen bonding and its nitrogen atoms with TYR422, SER545, THR500 and THR347, also via hydrogen bonding (Fig. 14). Gentamycin has a docking score of -3.996 kcal/mol and interacted with the amino acid residues of the receptor through its hydroxyl groups with THR343, GLN345 and TYR422 via hydrogen bonding while its nitrogen atoms interacted with THR343, THR500, SER545, also via hydrogen bonding (Fig. 15).

With the PBP-2 A receptor, 1VQQ for *S. aereus*, PDMA has a binding affinity of − 5.115 kcal/mol with interaction between it and the amino acid residues of the receptor at GLN292 from the hydrogen atoms on the hydrazine and amide groups via hydrogen bonding (Fig. 16), 5NS has a docking score of − 5.183 kcal/mol and interacted with the amino acid residues at GLU239 via the hydrogen atoms

on the hydrazine and amide groups (hydrogen bonding), ARG241 via the nitro oxygen (hydrogen bonding) and ARG151 from its hydroxyl oxygen via hydrogen bonding (Fig. 17). 4CN has a docking score of − 5.063 kcal/mol with interactions at GLN292 through its amide nitrogen via hydrogen bonding and with TYR272 via its phenyl ring due to pi-pi stacking (Fig. 18). Streptomycin has a docking score with the 6VBC (− 5.474 kcal/mol) while interacting through its carbonyl and hydroxyl oxygen atoms with GLU239, SER240 and ARG241 via hydrogen bonding and its nitrogen atoms with ASP275 and GLU170 via hydrogen bonding and salt bridge (Fig. 19). Gentamycin has a docking score of − 5.451 kcal/mol and interacted with the amino acid residues of the receptor through its oxygen atoms with ASP295, SER149, LYS148 and GLU239 via hydrogen bonding while its nitrogen atoms interacted
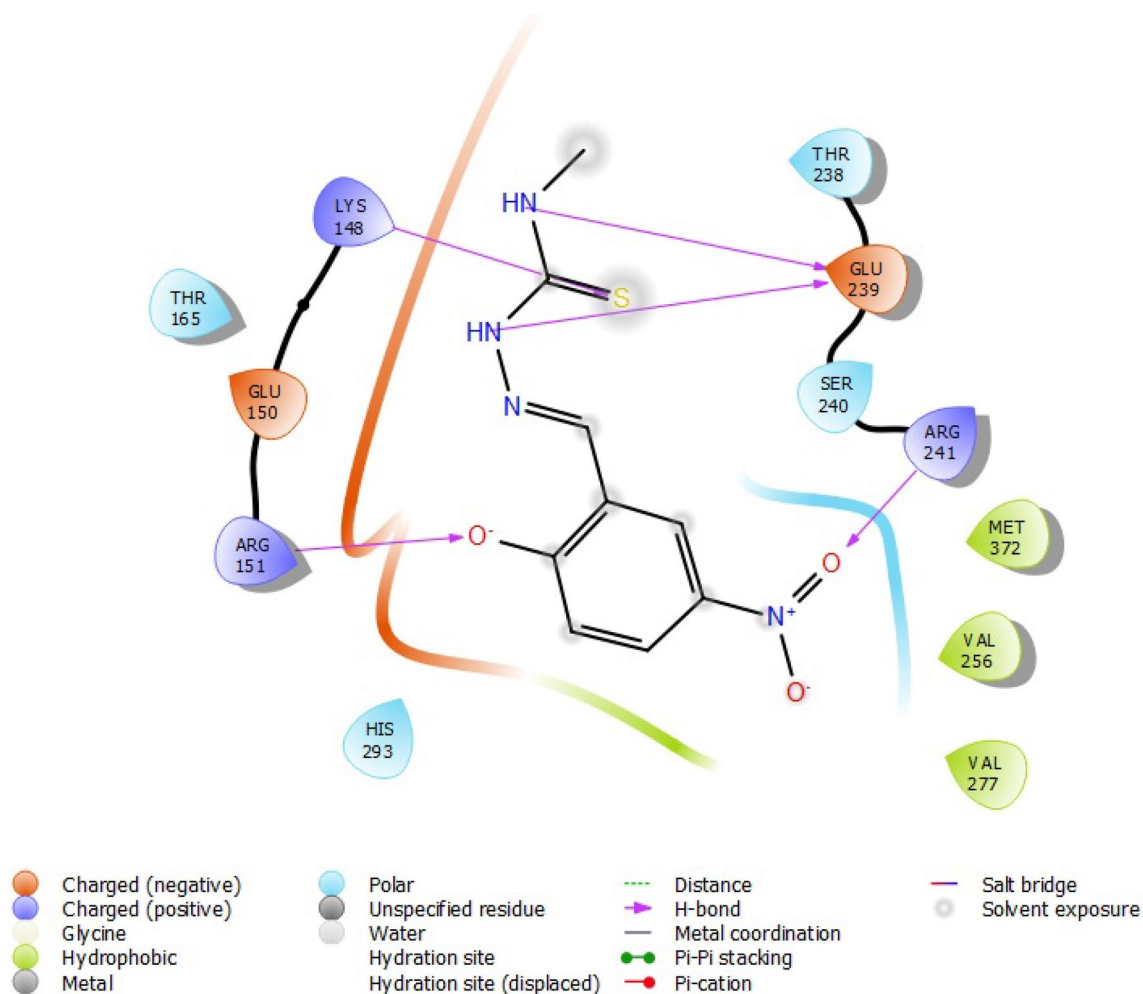
Fig. 17 5NS with 1VQQ

with HIS293 and ASP275 and also via hydrogen bonding and salt bridge (Fig. 20).

With the transcriptional regulator MvfR, 4JVI for *Pseudomonas spp*, PDMA has a binding affinity of -6.464 kcal/mol with interaction between it and the amino acid residues of the receptor at ARG209 from the hydrogen atoms on the hydrazine and amide groups via hydrogen bonding (Fig. 21), 5NS has a docking score of -5.895 kcal/mol and interacted with the amino acid residues at ARG209, also from the hydrogen atoms on the hydrazine and amide groups via hydrogen bonding (Fig. 22). 4CN has a docking score of -6.382 kcal/mol with interactions at ARG209 through its amide nitrogen via hydrogen bonding (Fig. 23).

Streptomycin has a docking score of -5.229 kcal/mol while interacting through its hydroxyl oxygen atoms with TYR258, ASN206 and ILE186 via hydrogen bonding and its nitrogen atoms with ILE186, ARG209, LEU207 and GLU151 via hydrogen bonding (Fig. 24). Gentamycin has a docking score of -7.069 kcal/mol and interacted with the amino acid residues of the receptor through its oxygen atoms with ASP264 and TYR258 via hydrogen bonding while its nitrogen atoms interacted with LEU207, ARG209 and GLU151 via hydrogen bonding and salt bridge (Fig. 25).

For the beta lactamase receptor, 4XUZ used for *Klebsiella spp*, PDMA has a binding affinity of – 5.028 kcal/mol with interaction between it and the amino acid residues of
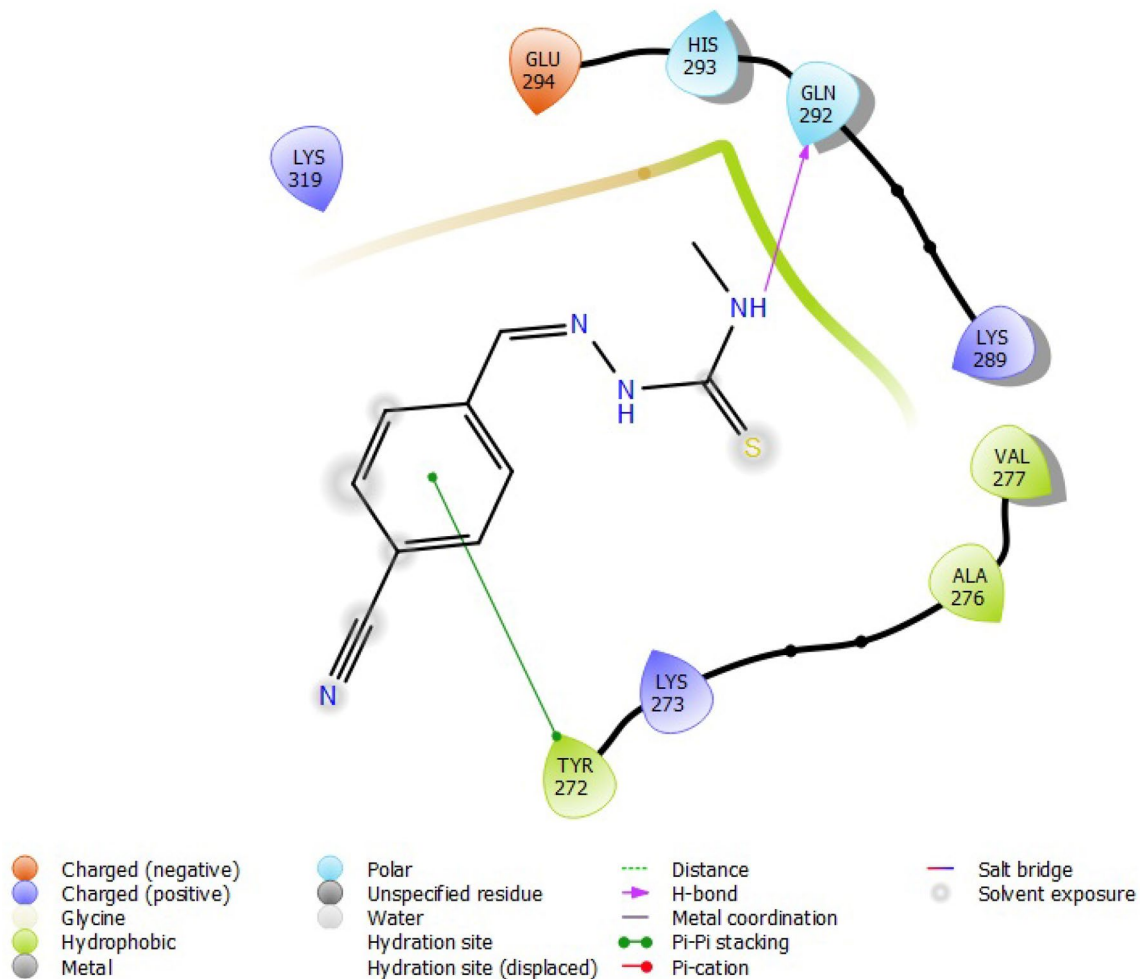
Fig. 18 4CN with 1VQQ

the receptor at GLY150 and ARG19 from the sulphur atom and imine nitrogen, respectively, via hydrogen bonding (Fig. 26), 5NS has a docking score of − 4.778 kcal/mol and interacted with the amino acid residues at GLN240 via its amide nitrogen (hydrogen bonding), THR239 via its hydrazine nitrogen (hydrogen bonding), ARG19 and ALA42 via its hydroxyl oxygen due to salt bridge and hydrogen bonding respectively (Fig. 27). 4CN has a docking score of − 4.691 kcal/mol with no visible interaction (Fig. 28).

Streptomycin has a docking score of − 3.988 kcal/mol while interacting through its hydroxyl oxygen atoms with GLY18 and GLY150 (hydrogen bonding) and via its nitrogen atom with GLU39 due to hydrogen bonding (Fig. 29). Gentamycin has a docking score of − 4.148 kcal/mol and interacted with the amino acid residues of the receptor through its oxygen atoms with GLU39 via hydrogen bonding while its nitrogen atoms interacted with GLU39 and GLY18 via hydrogen bonding and salt bridge (Fig. 30).
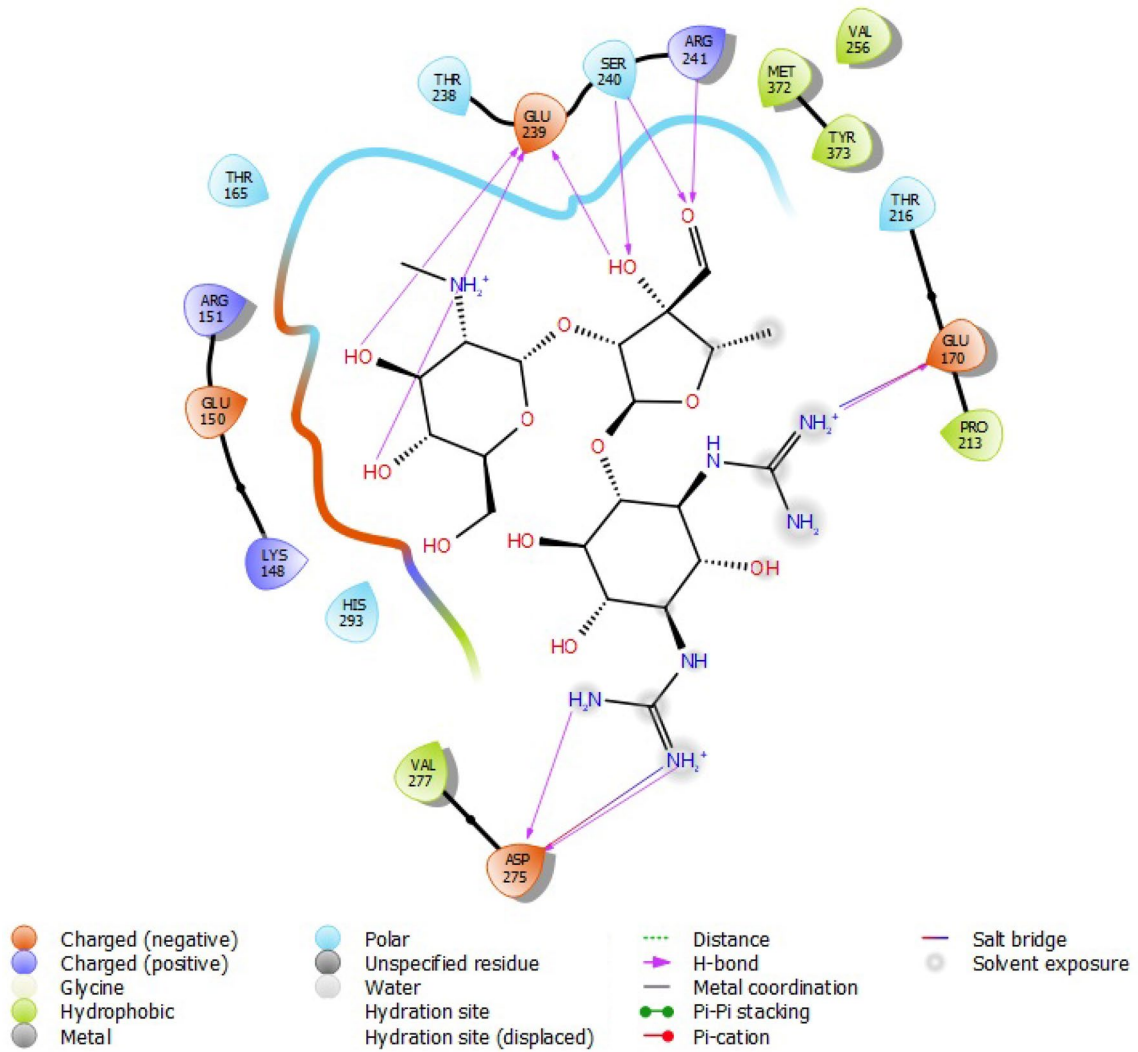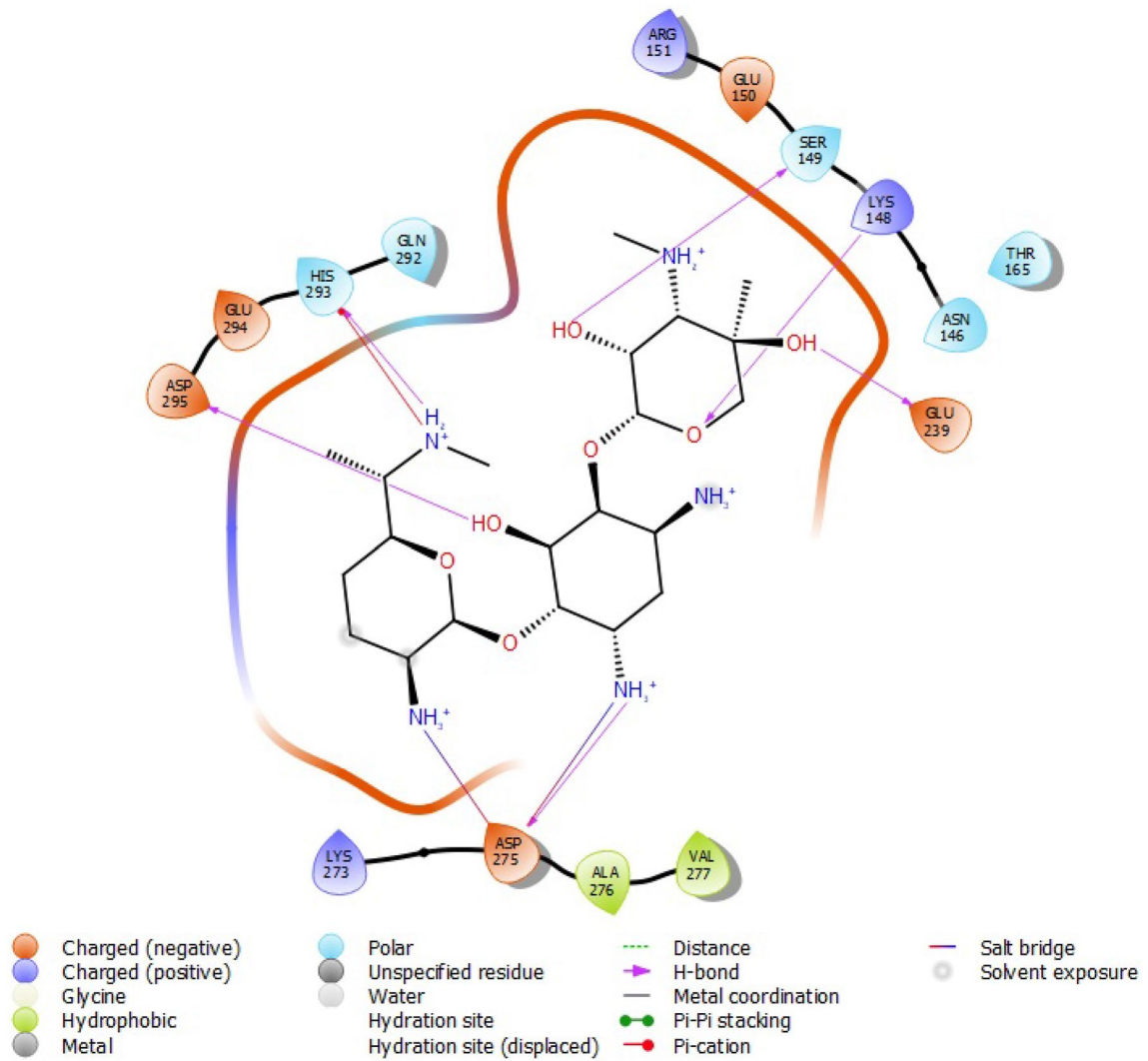
Fig. 19 Streptomycin with 1VQQ
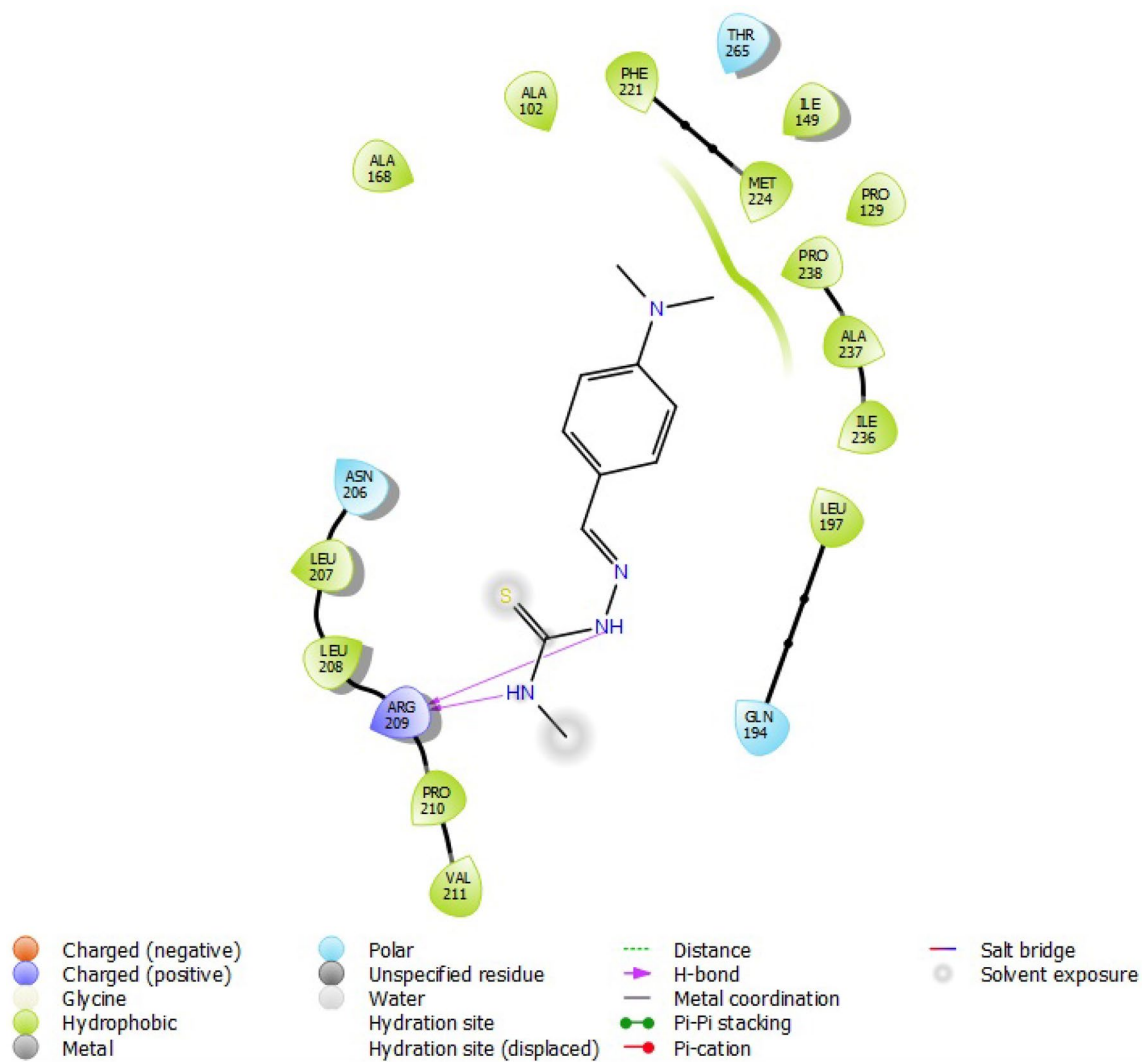
Fig. 20 Gentamycin with 1VQQ
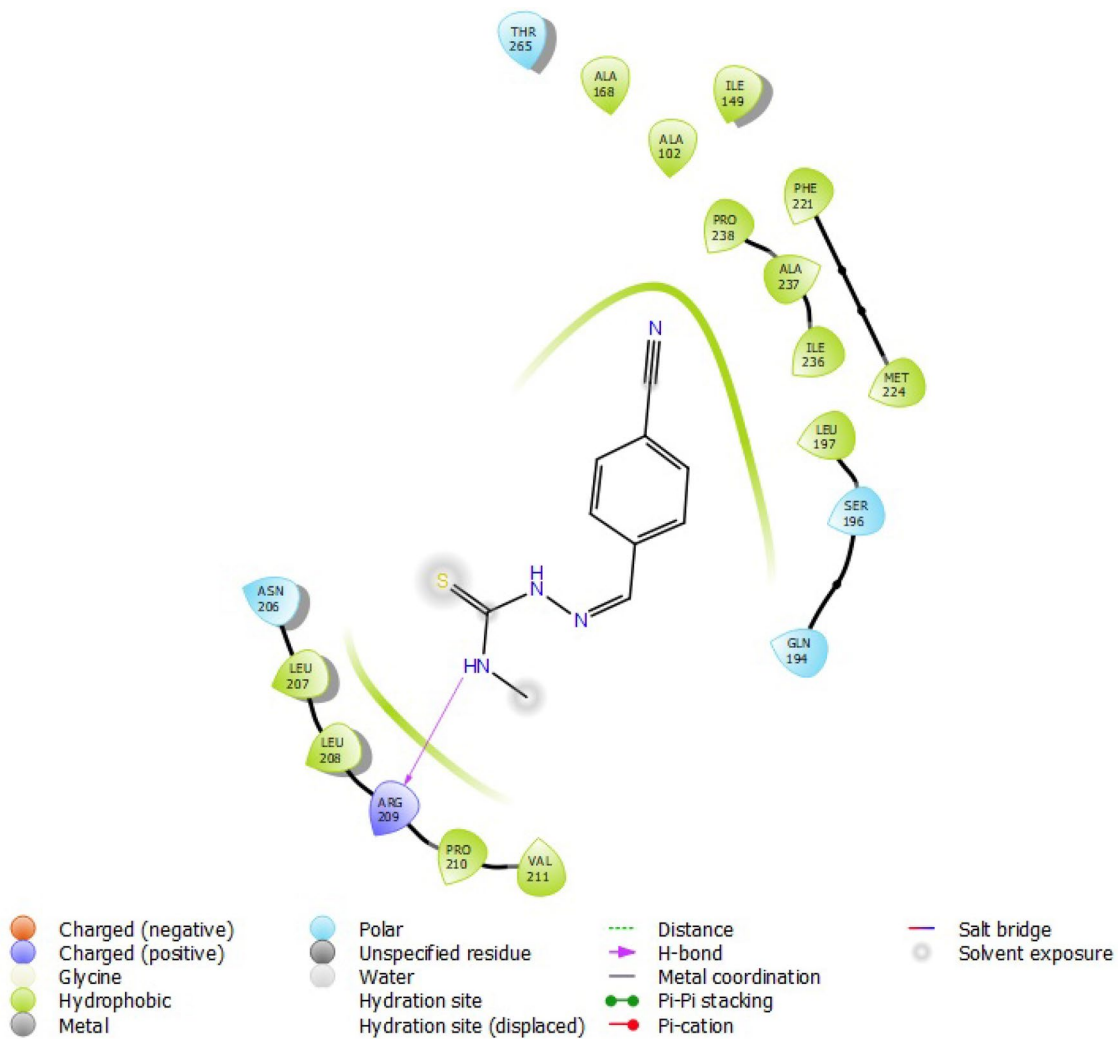
Fig. 21 PDMA with 4JVI

Fig. 22 5NS with 4JVI

● Charged (negative)	● Polar	---- Distance	— Salt bridge
● Charged (positive)	● Unspecified residue	➤ H-bond	○ Solvent exposure
○ Glycine	○ Water	— Metal coordination	
● Hydrophobic	Hydration site	●—● Pi-Pi stacking	
● Metal	Hydration site (displaced)	●—● Pi-cation	
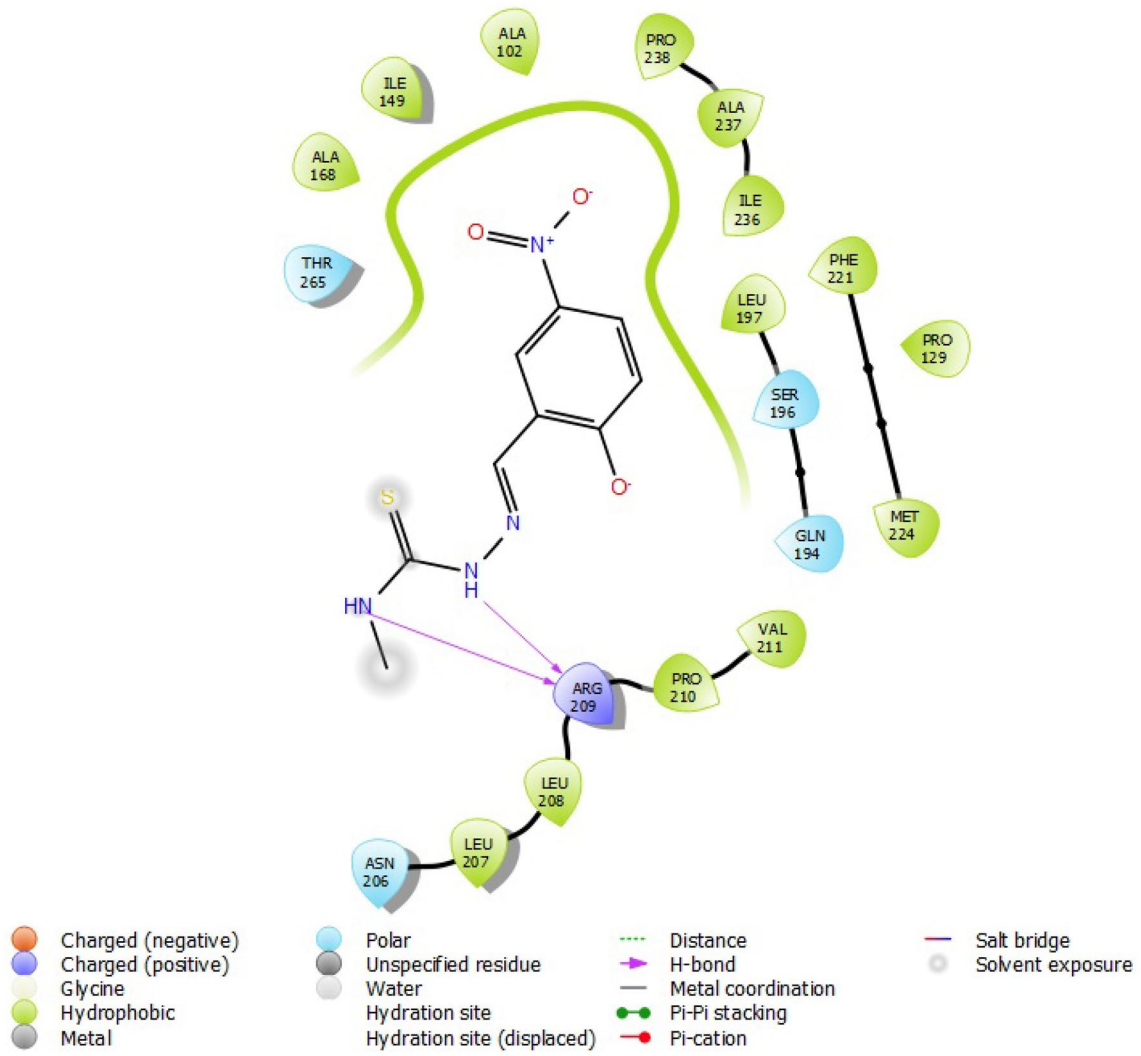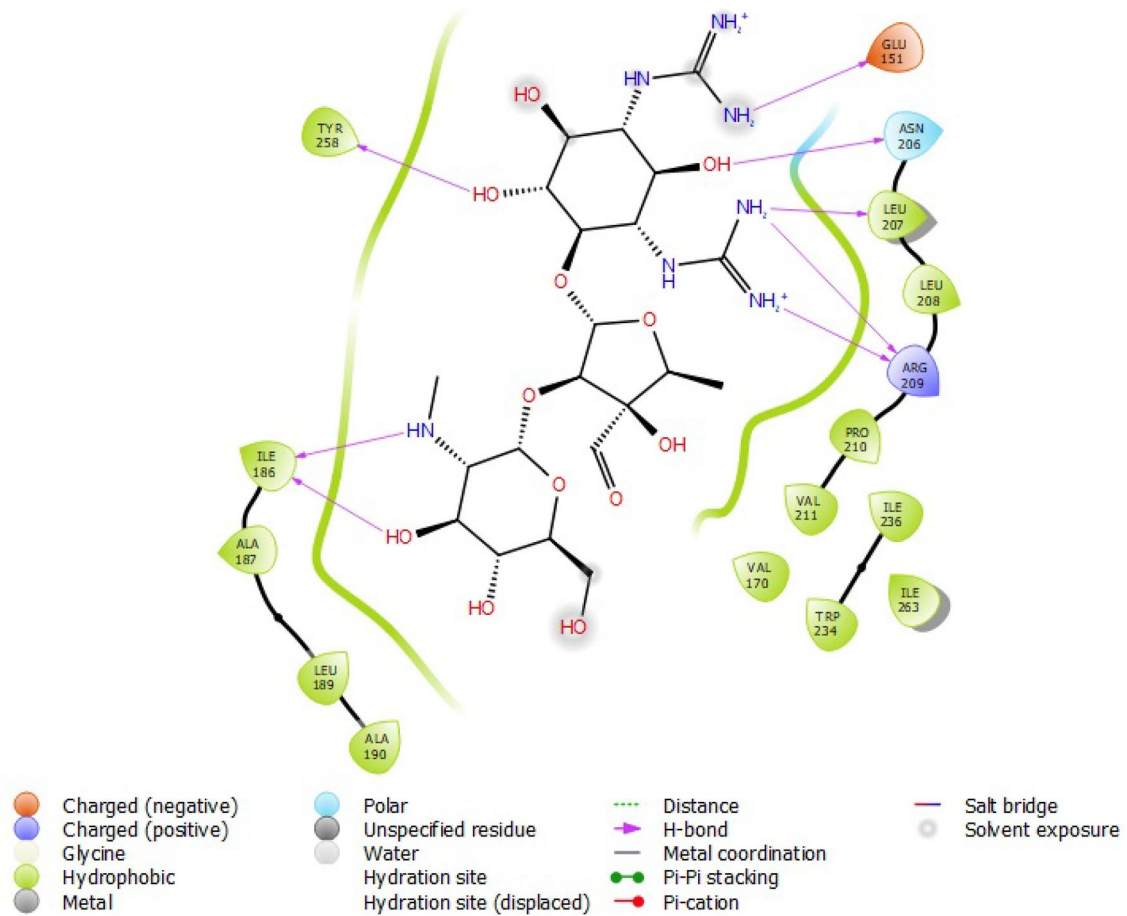
Fig. 23 4CN with 4JVI

Fig. 24 Streptomycin with 4JVI
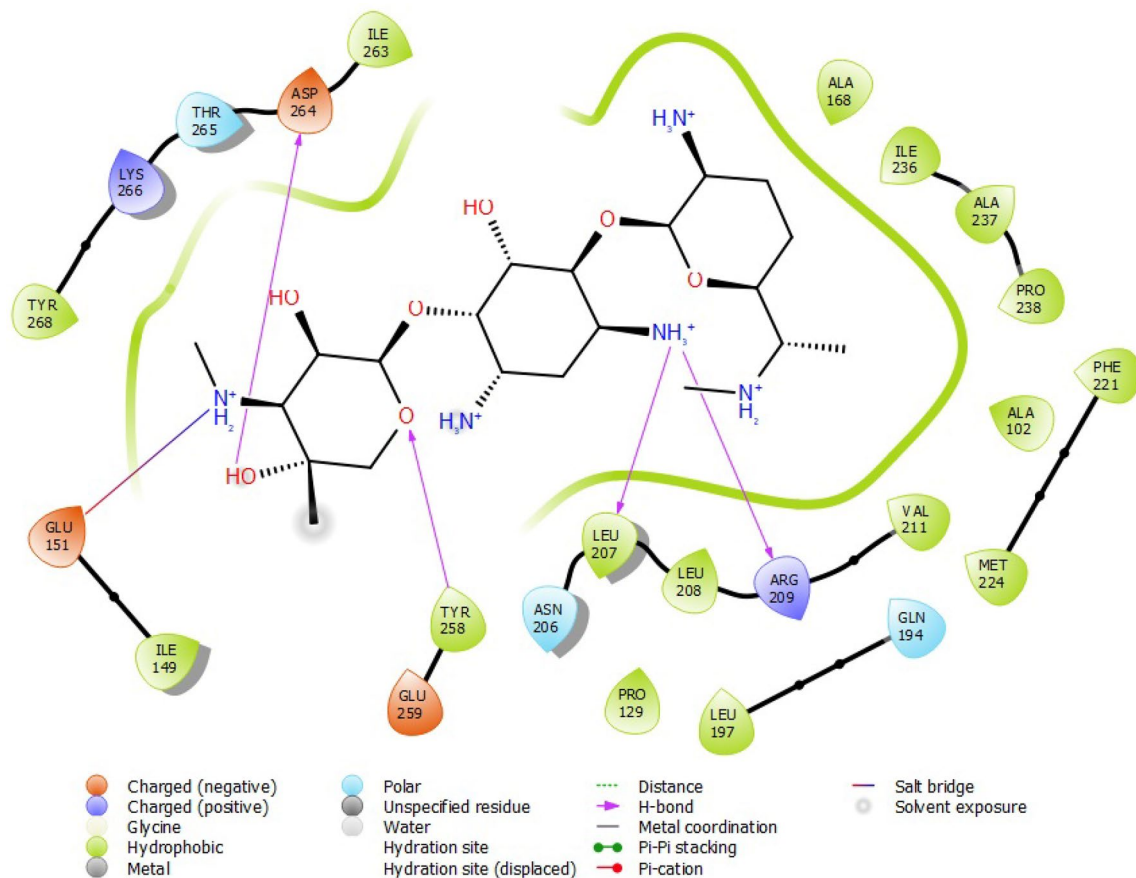
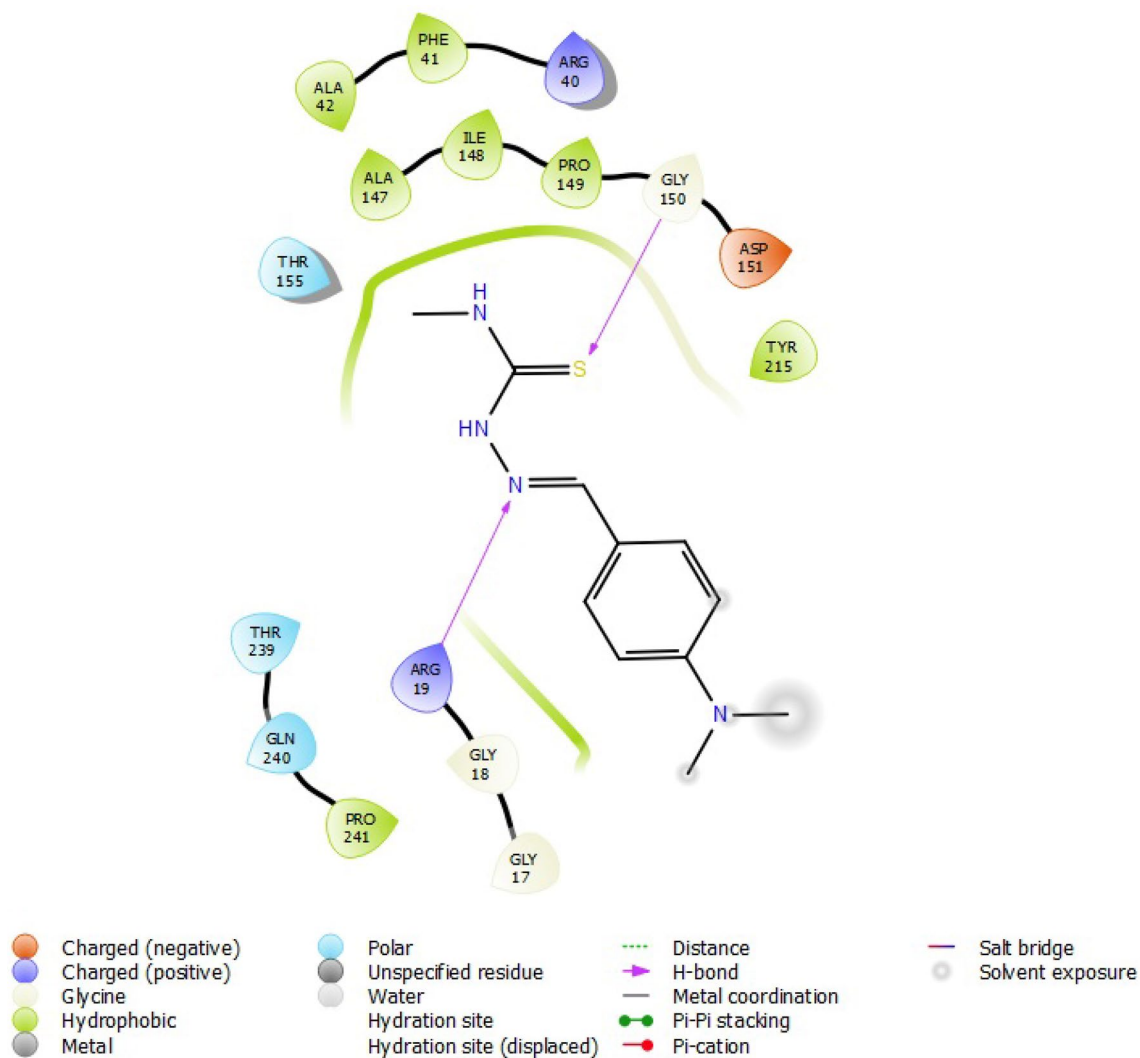**Fig. 25** Gentamycin with 4JVI

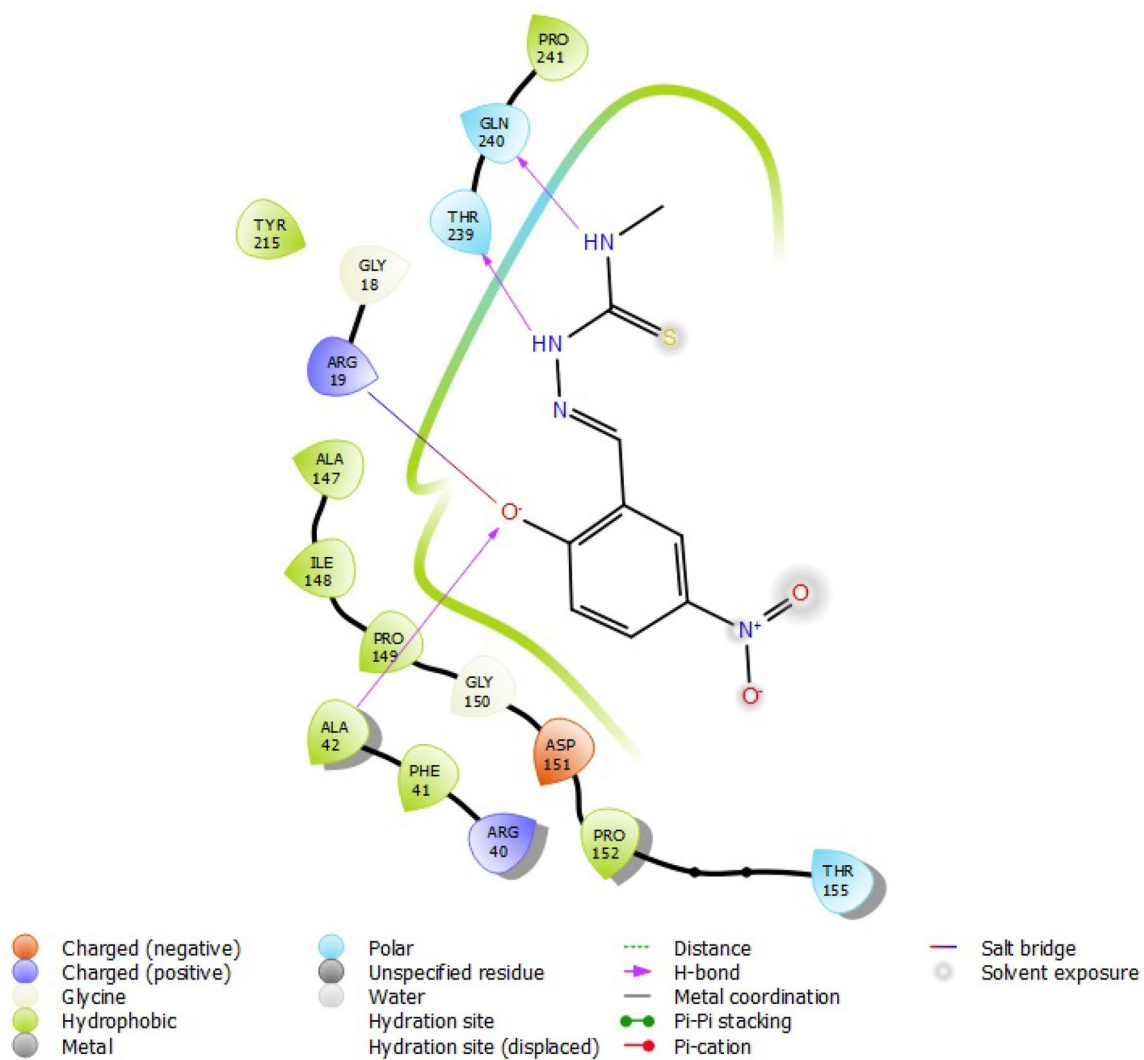**Fig. 26** PDMA with 4XUZ
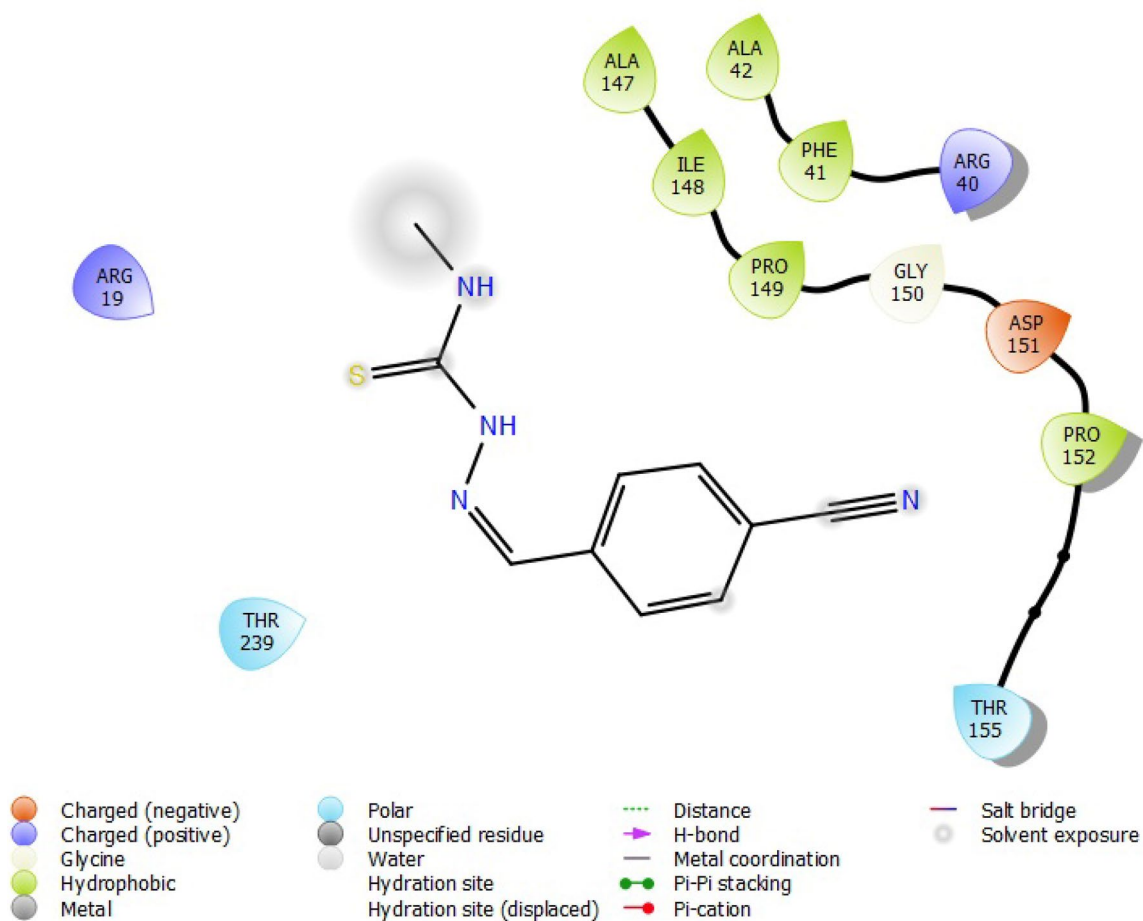
Fig. 27 5NS with 4XUZ
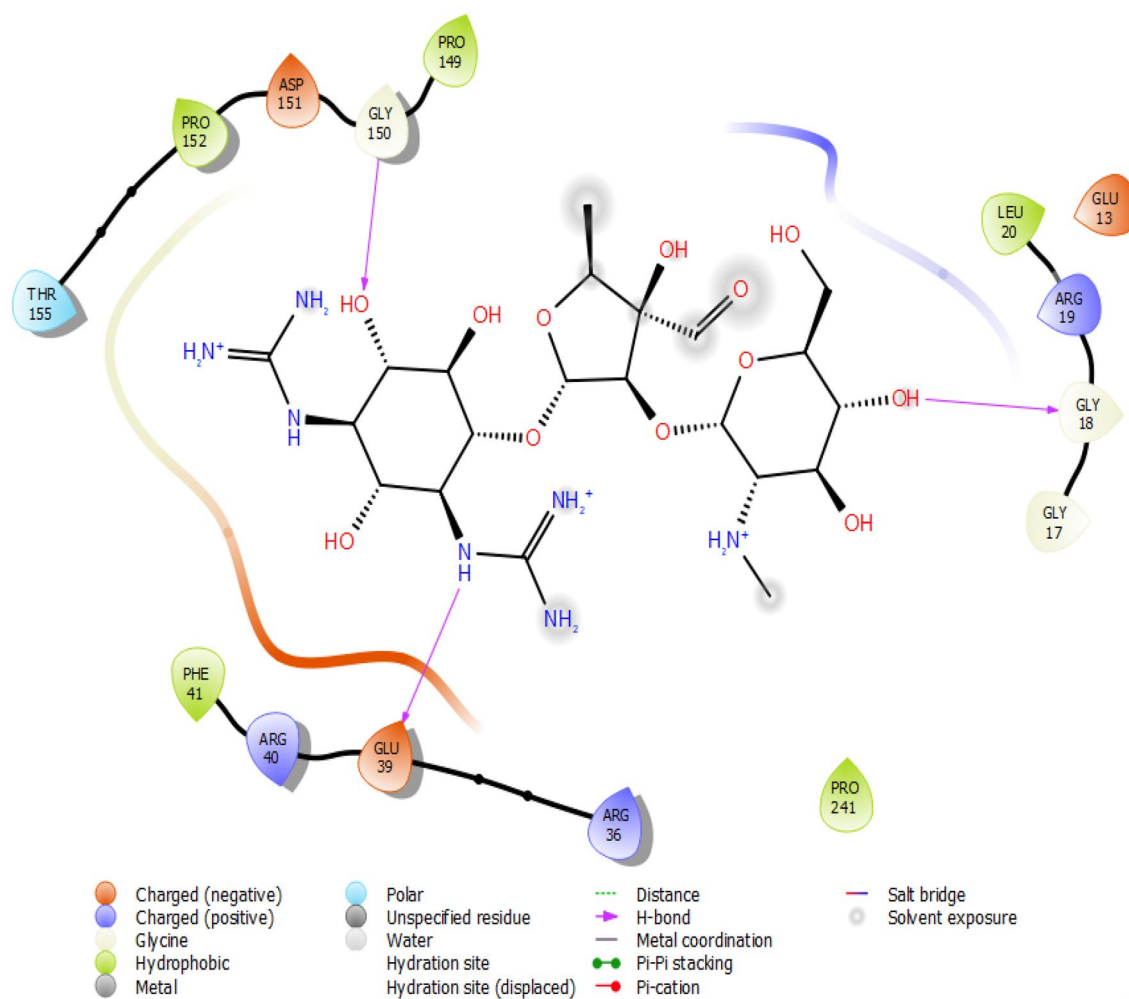
Fig. 28 4CN with 4XUZ
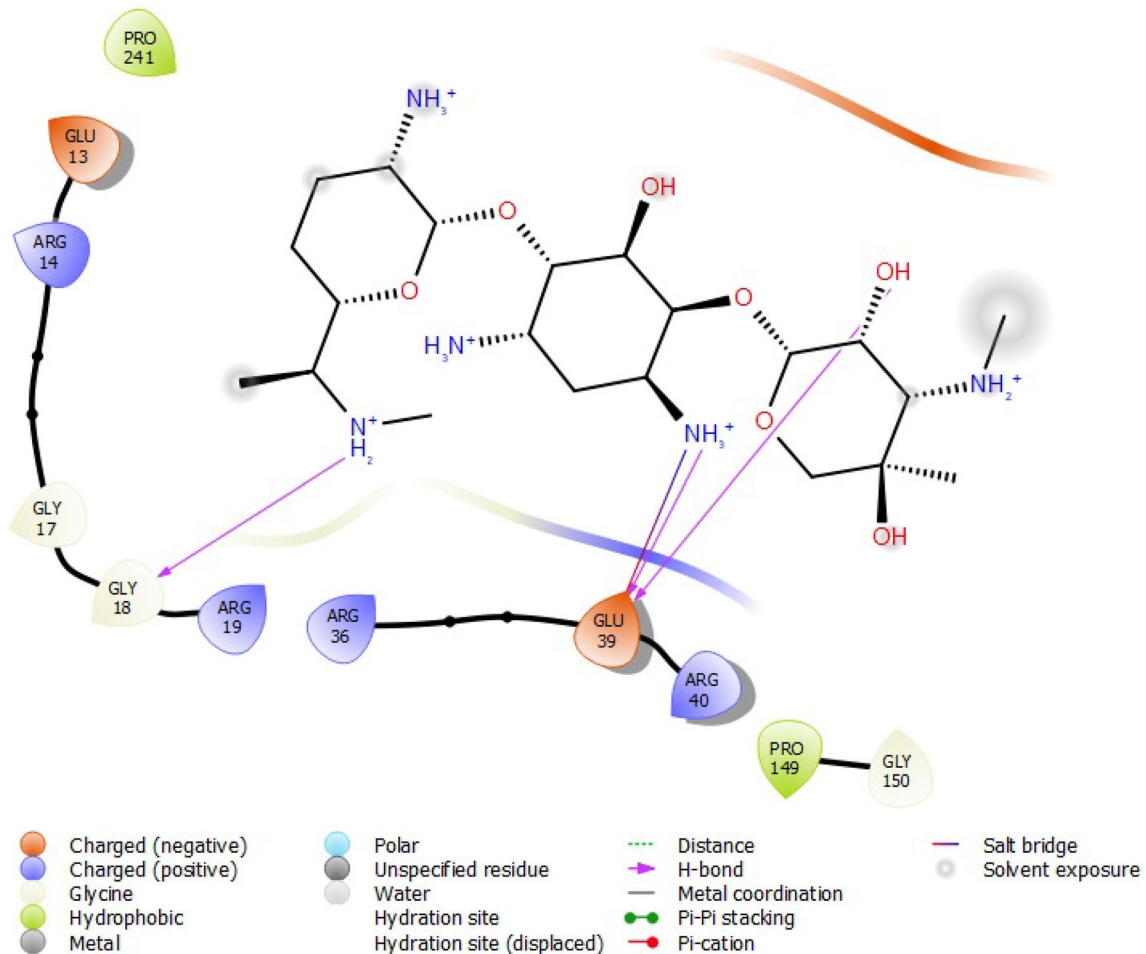
Fig. 29 Streptomycin with 4XUZ

Fig. 30 Gentamycin with 4XUZ

4 Conclusion

This work has presented the Schiff bases of synthesized thiosemicarbazone-benzaldehyde derivatives- PDM, 5NS and 4CN as potent antibacterial candidates/agents. The in-vitro antibacterial studies showed that 5NS and PDM were even more active than one of the standard drug streptomycin against the bacterial strains *Staphylococus aureus* and *Pseudomona aeruginosa* respectively while 5NS appeared to have the same activity with the strongest standard drug, gentamycin in the order PDMA < 4CN < Streptomycin < Gentamycin = 5NS against *Klebsiella pneumonia*. Additionally, the theoretical and molecular docking studies confirms the antibacterial activity of these molecules and also their ability to inhibit corrosion of metals in acidic media. The global and local reactivity descriptors revealed that these molecules can donate and at the same time accept electrons to the metals' surface and from metals' orbitals which suggests their potentials as corrosion inhibitors, which was also supported by their adsorption parameters on Fe(110).

Declarations

Conflict of interest All authors declare that there is no conflict of interest.

Open Access This article is licensed under a Creative Commons Attribution 4.0 International License, which permits use, sharing, adaptation, distribution and reproduction in any medium or format, as long as you give appropriate credit to the original author(s) and the source, provide a link to the Creative Commons licence, and indicate if changes were made. The images or other third party material in this article are included in the article's Creative Commons licence, unless indicated otherwise in a credit line to the material. If material is not included in the article's Creative Commons licence and your intended use is not permitted by statutory regulation or exceeds the permitted use, you will need to obtain permission directly from the copyright holder. To view a copy of this licence, visit http://creativecommons.org/licenses/by/4.0/.

References

1. Wang X, Ding G, Duan Y, Zhu Y, Zhu G, Wang M, Li X, Zhang Y, Qin X, Hung CH (2020) A novel triphenylamine-based bis-Schiff bases fluorophores with AIE-activity as the hydrazine fluorescence turn-off probes and cell imaging in live cells. Talanta 217:121029. https://doi.org/10.1016/j.talanta.2020.121029

2. Sadia M, Khan J, Naz R, Zahoor M, Shah SWA, Ullah R, Sohaib M et al (2021) Schiff base ligand L synthesis and its evaluation as anticancer and antidepressant agent. J King Saud Univ-Sci 33(2):101331

3. Abu-Dief AM, Mohamed IM (2015) A review on versatile applications of transition metal complexes incorporating Schiff bases. Beni-suef Univ J Basic Appl Sci 4(2):119–133

4. Przybylski P, Huczynski A, Pyta K, Brzezinski B, Bartl F (2009) Biological properties of schiff bases and azo derivatives of phenols. Curr Org Chem 13(2):124–148

5. Siddique M, Saeed AB, Dogar NA, Ahmad S (2013) Biological potential of synthetic hydrazide based Schiff bases. J Sci Innov Res 2:651–657

6. Garnovskii AD, Nivorozhkin AL, Minkin VI (1993) Ligand environment and the structure of Schiff base adducts and tetracoordinated metal-chelates. Coord Chem Rev 126(1–2):1–69

7. Walsh CT, Orme-Johnson WH (1987) Nickel enzymes. Biochemistry 26(16):4901–4906

8. Nayab S, Alam A, Ahmad N, Khan SW, Khan W, Shams DF, Lee H et al (2023) Thiophene-derived Schiff base complexes: synthesis, characterization, antimicrobial properties, and molecular docking. ACS Omega 8(20):17620–17633

9. Fabiyi FS, Olanrewaju AA (2019) Synthesis, characterization, thermogravimetric and antioxidant studies of New Cu(II), Fe(II), mn(II), Cu(II), zn(II), Co(II) and ni(II) complexes with benzoic acid and 4,4,4-Trifluoro-1-(2-naphthyl)-1,3-butanedione. Int J Chem 11(1):60–70

10. Khalil EA, Mohamed GG (2023) Synthesis and characterization of some transition and inner transition mixed ligand complexes derived from Schiff base ligand and o-aminophenol. Inorg Chem Commun 153:110825

11. Feizpour S, Hosseini-Yazdi SA, Safarzadeh E, Baradaran B, Dusek M, Poupon M (2023) A novel water-soluble thiosemicarbazone Schiff base ligand and its complexes as potential anticancer agents and cellular fluorescence imaging. J Biol Inorg Chem. https://doi.org/10.1007/s00775-023-02001-5

12. Oke DG, Faboro EO, Olanrewaju AA, Oyeneyin OE, Lajide L (2022) In vitro antifungal and in-silico antibacterial evaluations of anacardic acid and its complexes from cashew nut shell oil. Trop J Nat Prod Res 6(8):1290–1296

13. Catalano A, Iacopetta D, Ceramella J, Scumaci D, Giuzio F, Saturnino C, Sinicropi MS (2022) Multidrug resistance (MDR): a widespread phenomenon in pharmacological therapies. Molecules 27(3):616

14. Iacopetta D, Catalano A, Ceramella J, Saturnino C, Salvagno L, Ielo I, Drommi D, Scali E, Plutino MR, Rosace G et al (2021) The different facets of triclocarban: a review. Molecules 26(9):2811

15. Li YX, Erhunmwunsee F, Liu M, Yang K, Zheng W, Tian J (2022) Antimicrobial mechanisms of spice essential oils and application in food industry. Food Chem 382:132312

16. Jubair N, Rajagopal M, Chinnappan S, Abdullah NB, Fatima A (2021) Review on the antibacterial mechanism of plant-derived compounds against multidrug-resistant bacteria (MDR). Evid-Based Complement Altern Med. https://doi.org/10.1155/2021/3663315

17. Magryś A, Olender A, Tchórzewska D (2021) Antibacterial properties of Allium sativum L. against the most emerging multidrug-resistant bacteria and its synergy with antibiotics. Arch Microbiol 203:2257–2268

18. Beraldo H, Gambino D (2004) Wide pharmacological versatility of semicarbazones, thiosemicarbazones and their metal complexes. Mini-Rev Med Chem 4:159–165

19. Shakya B, Yadav PN (2020) Thiosemicarbazones as potent anticancer agents and their modes of action. Min Rev in Med Chem 20(8):638–661

20. Thanh ND, Duc HT, Duyen VT, Tuong PM, Van Quoc N (2015) Synthesis and antibacterial and antifungal activities of N-(tetra-O-acetyl-β-d-glucopyranosyl) thiosemicarbazones of substituted 4-formylsydnones. Chem Cent J 9:1–14

21. de Assis DRR, Oliveira AA, Porto SL, Rabelo RAN, Lages EB, Santos VC, Machado FS (2021) 4-Chlorophenylthioacetone-derived thiosemicarbazones as potent antitrypanosomal drug candidates: investigations on the mode of action. Bioorg Chem 113:105018

22. Sharma N, Pal Pathak D (2017) Synthesis and characterization of novel benzaldehyde thiosemicarbazones and evaluation of their antibacterial. Antifung Antioxid Act IJPSR 8(2):667–678

23. Doğan M, Koçyiğit ÜM, Gürdere MB, Ceylan M, Budak Y (2022) Synthesis and biological evaluation of thiosemicarbazone derivatives. Med Oncol 39(10):157

24. Ramalingam A, Sambandam S, Medimagh M, Al-Dossary O, Issaoui N, Wojcik MJ (2021) Study of a new piperidone as an anti-alzheimer agent: molecular docking, electronic and inter-molecular interaction investigations by DFT method. J King Saud Univ-Sci 33(8):101632

25. Mohapatra RK, Dhama K, El-Arabey AA, Sarangi AK, Tiwari R, Emran TB, Abdalla M et al (2021) Repurposing benzimidazole and benzothiazole derivatives as potential inhibitors of SARS-CoV-2: DFT, QSAR, molecular docking, molecular dynamics simulation, and in-silico pharmacokinetic and toxicity studies. J King Saud Univ-Sci 33(8):101637

26. Olanrewaju AA, Fabiyi FS, Ibeji CU, Kolawole EG, Gupta R (2020) Synthesis, spectral, structure and computational studies of novel transition Metal (II) complexes of (Z)-((dimethylcarbamothioyl) thio)((1,1,1-trifluoro-4-(naphthalen-2-yl)-4-oxobut-2-en-2-yl) oxy). J Mol Struct 1211(2020):128057. https://doi.org/10.1016/j.molstruc.2020.128057

27. Kistan A, Anna Benedict B, Vasanthan S, PremKumar A, Kullappan M, Ambrose JM, Surapaneni KM (2021) Structure-based virtual screening of benzaldehyde thiosemicarbazone derivatives against DNA gyrase B of *Mycobacterium tuberculosis*. Evidence-Based Complement Altern Med 2021:1–11

28. Olanrewaju AA, Ibeji CU, Oyeneyin OE (2020) Biological evaluation and molecular docking of some newly synthesized 3d-series metal(II) mixed-ligand complexes of fluoro-naphthyl diketone and dithiocarbamate. SN Appl Sci 2(4):678

29. Oyeneyin OE, Ojo ND, Ipinloju N, James AC, Agbaffa EB (2022) Investigation of corrosion inhibition potentials of some aminopyridine Schiff bases using density functional theory and Monte Carlo simulation. Chem Afr 5(2):319–332

30. Becke AD (1993) Density-functional thermochemistry III the role of exact exchange. J Chem Phys 98(7):5648–5652

31. Shao JYY, Molnar LF et al (2014) SPARTAN 14', build 1.01. Wavefunction Inc., Irvine

32. Obi-Egbedi NO, Ojo ND (2015) Computational studies of the corrosion inhibition potentials of some derivatives of 1H-Imidazo[4,5-F][1,10] phenanthroline. J Sci Res 14:50–56

33. Akinyele OF, Adekunle AS, Olayanju DS, Oyeneyin OE, Durodola SS, Ojo ND, Akinmuyisitan AA, Ajayeoba TA, Olasunkanmi LO (2022) Synthesis and corrosion inhibition studies of (E)-3-(2-(4-chloro-2-nitrophenyl)diazenyl)-1-nitrosonaphthalen-2-ol on mild steel dissolution in 0.5 M HCl solution- experimental, DFT and Monte Carlo simulations. J Mol Struct 1268:133738. https://doi.org/10.1016/j.molstruc.2022.133738)

34. Oyeneyin OE, Ojo ND, Ipinloju N, Agbaffa EB, Emmanuel AV (2022) Investigation of the corrosion inhibition potentials of some 2-(4 (substituted)arylidene)-1H-indene-1,3-dione derivatives: density functional theory and molecular dynamics simulation. Beni-Suef Uni J Bas Appl Sci 11(1):1–14

35. Oyeneyin OE (2023) DFT and monte carlo simulations on the corrosion inhibitive potentials of some furan-based carbohydrazide derivatives. Lett Appl NanoBioSci 12(4):1–22

36. Akinyele OF, Adekunle AS, Olayanju DS, Oyeneyin OE, Durodola SS, Ojo ND, Akinmuyisitan AA, Ajayeoba TA, Olasunkanmi LO (2022) Synthesis and corrosion inhibition studies of (E)-3-(2-(4–chloro-2-nitrophenyl)diazenyl)-1-nitrosonaphthalen-2-ol on mild steel dissolution in 0.5 M HCl solution-experimental, DFT and Monte Carlo simulations. J Mol Str 1268:133738

37. Schrödinger L (2018) Schrödinger Release 2018–1: maestro. Schrödinger LLC

38. Madhavi Sastry G, Adzhigirey M, Day T, Annabhimoju R, Sherman W (2013) Protein and ligand preparation: parameters, protocols, and influence on virtual screening enrichments. J Comput Aided Mol Des 27(3):221–234

39. Schrödinger (2023) Release 2023-2: LigPrep, Schrödinger, LLC, New York

40. Shi L, Ge HM, Tan SH, Li HQ, Song YC, Zhu HL, Tan RX (2007) Synthesis and antimicrobial activities of Schiff bases derived from 5-chloro-salicylaldehyde. Eur J Med Chem 42(4):558–564

41. Wang M, Tran JH, Jacoby GA, Zhang Y et al (2003) Plasmid-mediated quinolone resistance in clinical isolates of Escherichia coli from Shanghai China. Antimicrob Agents Chemother 47(7):2242–2248

42. Akintemi EO, Govender KK, Singh T (2022) A DFT study of the chemical reactivity properties, spectroscopy and bioactivity scores of bioactive flavonols. Comp Theo Chem 1210:113658

43. Waziri I, Yusuf TL, Akintemi EO, Kelani MT, Muller A (2023) Spectroscopic, crystal structure, antimicrobial and antioxidant evaluations of new Schiff base compounds: an experimental and theoretical study. J Mol Str 1274:134382

44. Ibeji CU, Akintayo DC, Oluwasola HO, Akintemi EO, Onwukwe OG, Eziomume OM (2022) Synthesis, experimental and computational studies on the anticorrosion performance of substituted Schiff bases of 2methoxybenzaldehyde for mild steel in HCl medium. Sci Rep 13(1):3265

Publisher's Note Springer Nature remains neutral with regard to jurisdictional claims in published maps and institutional affiliations.